Spring 2013

Parametric investigation of strain gauges in structural damage detection

Matthew Francis Anderson
University of Iowa

PARAMETRIC INVESTIGATION OF STRAIN GAUGES IN STRUCTURAL DAMAGE DETECTION

by

Matthew Francis Anderson

A thesis submitted in the partial fulfillment
of the requirements for the
Master of Science degree in Civil and Environmental Engineering
(Structural Engineering) in the Graduate College of
The University of Iowa

May 2013

Thesis Supervisor: Associate Professor Salam Rahmatalla

Graduate College
The University of Iowa
Iowa City, Iowa

CERTIFICATE OF APPROVAL

_____

MASTER'S THESIS

_____

This is to certify that the Master's thesis of

Matthew Francis Anderson

has been approved by the Examining Committee for the thesis requirement for the Master of Science degree in Civil and Environmental Engineering (Structural Engineering) at the May 2013 graduation.

Thesis Committee: _____
Salam Rahmatalla, Thesis Supervisor

_____
Colby Swan

_____
M. Asghar Bhatti

ACKNOWLEDGEMENTS

I would like to thank the Civil & Environmental Engineering faculty and staff at the University of Iowa for helping me during my time as a student. Acknowledgement should also be given to Charles Schallhorn for assisting me and providing answers to all of my myriad of questions. Finally, I would like to especially thank my advisor, Associate Professor Salam Rahmatalla, for giving me the opportunity to complete this research, and for guiding me with patience during my graduate studies.

Most importantly, I would like to thank my family and loved ones for supporting me in my education with understanding and confidence.

ABSTRACT

Vibration-based damage detection (VBDD) methods are used to detect damage in structural members non-evasively. This investigation began with two objectives: to prove a VBDD method could detect damage using strain gauges both analytically and experimentally, and to then use that method to determine the distance from a damaged area that strain gauges could be effective. Work began simultaneously using finite element software and physical experiments. It was determined that a VBDD method could detect damage with strain gauges in both settings. A parametric study was then completed that used probabilistic methods to identify an effective range for strain gauges over the length of the structural member.

TABLE OF CONTENTS

LIST OF TABLES

LIST OF FIGURES

PREFACE

With the continual rise in the number of deficient bridges in the United States, more efficient damage detection methods are needed. Dynamic-based damage detection methods have shown promising success and potential for field applications. This method can be accomplished using different types of sensors, including transducers for acceleration, velocity, and displacement; however, strain gauges offer several advantages over these options. This study means to utilize these advantages in the investigation. The objective of this study is to complete a parametric investigation in order to identify the effectiveness and the useful range of strain gauges for dynamically detecting damage in a steel member.

Tests are completed using both finite element models and laboratory experiments to identify the effective range of strain gauges around the damaged area. Using the finite element model, a range is identified where strain gauges could be used to effectively detect damage in the beam. A new probabilistic methodology is introduced to quantify damage in the beam based on the changes in its dynamic properties, represented by the frequency response function (FRF) between a response signal and a reference signal. This probabilistic method concludes that an effective range for detecting and quantifying the damage can be established.

CHAPTER 1: INTRODUCTION

1.1 Motivation

According to the U.S. Department of Transportation Federal Highway Administration (FHWA) in 2011, slightly more than 600,000 bridges in the U.S. territories were considered either structurally deficient or functionally obsolete. This data includes 24,537 bridges listed for the State of Iowa, giving it the 6th most among the list of states. It was also estimated that in order to repair all deficient bridges over the next 50 years, an investment of $850 billion (2006 USD) would be needed.

This high need of repairs, coupled with the major investment needed for these repairs, makes a reliable damage detection system valuable. It would allow states and agencies the ability to accurately rank the importance of repairs, thus using their funds more efficiently. A vibration-based damage detection (VBDD) system improves on other damage detection systems, such as acoustic, ultrasonic, radiography, or magnetic field methods, by addressing two common limitations: the location of the damage must be known prior to testing and must be readily accessible [1]. Of course, VBDD would also improve on the original damage detection of human inspectors manually searching the structure.

Many studies over the 30 years of investigating VBDD have produced systems that are capable of identifying damage after it has occurred [2]. Most current systems are also, to a certain degree, able to localize, or identify the location of, the damage. However, a majority of the systems utilized accelerometers as the source for the data. While VBDD systems that utilize accelerometers are accurate in identifying the vibrations throughout the bridge, it is often expensive to outfit the entire bridge with them. Therefore, less expensive monitors, such as strain gauges, would be more practical if they were able to operate as well as accelerometers. Strain gauges also have the benefit of being able to detect damage both dynamically and statically.

1.2 Background

Using vibrations to detect damage in structures is not a recent phenomenon, but instead has been researched in the last several decades. In fact, changes in the natural frequencies of the system were being used in this capacity in the late 1970's [2]. Some methods include, but are not limited to: frequency response functions (FRF), neural networks, mode shapes, and dynamic flexibility. Although these methods differ in many areas, they are all similar in their basic premise; damage in the structure causes a change in certain characteristics, such as the mass and stiffness of the system. These in turn alter the measured dynamic characteristics, such as the natural frequencies and mode shapes.

Currently practiced methods of damage detection are mostly manual and local. Examples of these methods include acoustic, ultrasonic, magnetic-field methods, radiograph, eddy-current methods, and thermal fields. These differ from VBDD based on the coverage area, accessibility, and depth of inspection. Damage inside a beam or located on a part not easily viewed would still be detected using VBDD. Because of these deficiencies, several of these current analysis methods should be used simultaneously.

The method used for this study, the frequency response function (FRF) method, is an analysis tool that can be used for both existing structures and finite-element models. It is based on the comparison of the input excitation signal to the output measured signal for a structure before and after damage. Theoretically, the damage would cause changes in the natural frequency of the structure, thus producing a different measured output signal.

The FRF method is based on multiple assumptions that are considered valid for real-life conditions. First, as mentioned before, it assumes that damage will cause a change in the output dynamic characteristics (natural frequencies, damping, and vibration modes). This would be due to the damage causing a reduction in the stiffness of the structure, an experimentally-corroborated assumption [3]. Because natural frequencies depend on both stiffness and mass, the mass was considered and then assumed constant

for the entire experiment [2]. The damage-induced cracks would not decrease the mass noticeably compared with the entire mass of the structure.

The use of FRF outputs to detect damage depends somewhat on the device used to collect the signals. These usually are accelerometers, displacement transducers, or strain gauges. Because this study conducted most of the findings using strain gauges, these will be the only devices discussed. As is common in most studies, accelerometers were used to corroborate the data in the laboratory setting [4] [5].

A study, published in 1995 by Swamidas et al., detailed a comparison of damage detection between accelerometers, displacement transducers, and strain gauges. They used a finite element model of a cantilever plate with a crack increasing in depth to replicate damage. This study concluded accelerometers were able to detect damage globally in a system, but they were not able to localize the damage. To accomplish the localization, strain was monitored at three locations away from the damaged cross-section. It was stated that the change in modal parameters was most significant around the damaged area. Most importantly, it was found that damage could not be accurately detected using a shift in the natural frequencies; instead, the change in amplitude of the resonance peaks were much better at detecting damage. The closer to the damage, the more the amplitude of the peaks changed. The researchers also found that clearer information was provided when the strain gauges were used dynamically as opposed to statically.

Other studies, such the 1993 study by Chen et al., performed similar strain-based damage detection investigations and also concluded that damage could be detected using a VBDD. Again, the strain frequency response function was monitored for any change in amplitude, which would indicate damage. Unlike the previous study, this was carried out using a scaled model of an oil rig. Strain gauges were attached, and a saw cut was made near these gauges. Damage was detected both dynamically and statically. It was stated that the static damage detection was available because the crack affected not only the

stiffness and damping, but also the strain in the member close to the damage. A finite element model was created that validated, to a degree, the findings of the scaled model. One reason given for the discrepancy was that the analytical model did not take into account the frictional damping that would be present in a true crack. Overall, it was concluded that the strain FRF's had very noticeable changes as the damage increased.

As mentioned previously, VBDD is available for several different types of signals. In a 1996 study by Yam et al., a relationship between the displacement function and the strain function was derived. Because the strain FRF expression required several unknown variables, the authors stated they would determine the variables experimentally, thus avoiding the complex issue of solving for them. The study then experimentally tested an aluminum plate and calculated the FRF's using displacement and strain. It was concluded that there was little change for the displacement FRF's between a normal plate and a plate with a hole in it. However, the strain FRF's were able to detect and localize the hole in the plate. It was warned that the sensitivity and accuracy of the experimental data for the strain FRF's relied heavily on the equipment used to extract data. Due to this, the higher frequencies for the strain gauges were not as accurate as for the displacement FRF's.

Other studies conducted found similar issues and other disadvantages with using strain gauges dynamically. The most pressing issue was the presence of noise in the experimental signals and how this could distort the readings [6] [7]. In their 2008 study, Jang et al., mentioned that their findings would have improved significantly had the strain resolution improved from 1 microstrain to .001 microstrain. However, because foil strain gauges were chosen, the investigation was limited. The study also stated that using semiconductor strain gauges, as opposed to the standard wire or foil gauges, could increase their experiments' gauge factors from 20 to 100 times that of the other gauge versions. However, these semiconductor gauges' gauge factor (GF) could vary more from the stated value given by the manufacturer. This given variable, used in experiments to

calibrate the data-acquisition system, could fluctuate as much as ±5%. For foil gauges, the typical fluctuation is much smaller at ±.5%. The study then mentioned that grounding was an important issue, especially to reduce noise around 50 Hz. Other sources of error the study listed were from the lead wires and the cement used to bond the gauges to the specimen.

There are other VBDD methods that are not discussed in this study, but they all have a common trait; they are not used widespread in a practical environment to detect damage in structures. This is based on their perceived unreliability to detect unnoticeable damage. Damage identification has been given four benchmarks for a successful system, with each being more difficult than the previous one. They are: (1) Identifying damage existence, (2) Benchmark 1 plus the location of damage, (3) Benchmark 2 plus the severity and extent of damage, and (4) Benchmark 3 with the structural health and remaining capacity of the structure. Out of these, only the first three have been achieved, with most occurring with the first two benchmarks [8]. Research has been completed in the past that has tried to combine the advantages of multiple methods, such as using both accelerometers and strain gauges, to be able to complete the third benchmark [5].

1.3 Objective

The objective of this research was to conduct a parametric study to identify a useful range for strain gauges' locations around prone-to-damage areas to dynamically detect and quantify damage using numerical and experimental approaches. The strain frequency response function was used to determine how the dynamic properties of the structure changes as damage progresses. Validation in a laboratory setting was to be completed in order to compare data to the analytical model. The final product was to show how far from the damage a strain gauge would be useful.

CHAPTER 2: THEORY

The concept of an FRF signal can be demonstrated by the equation of motion of a single-degree-of-freedom mass-system with forced vibration. The left-side of Equation 1 has mass (m), damping coefficient (c), and stiffness (k). The right-side of the equation, F(t), is assumed to be an harmonic function.

(1) $$m\ddot{x} + c\dot{x} + kx = \mathrm{F(t)}$$

In order to obtain the true frequency response function, the equation of motion can be solved using a transformed solution, such as with Laplace transforms. The solution using these transforms is given in Equation 2.

(2) $$X(s) = \frac{F_0 s}{(ms^2+cs+k)(s^2+\omega_{dr}^2)}$$

If X(s), the Laplace transform of the output signal, is divided by F(s), the Laplace transform of the driving force, the frequency response function, H(s), is obtained. This ratio is important for several reasons, but one of the most basic is the ability to identify natural frequencies. At these frequencies, the displacement increases dramatically, thus increasing the FRF. Therefore, any peaks in an FRF signal are considered potential natural frequencies.

(3) $$\frac{X(s)}{F(s)} = \frac{1}{ms^2+cs+k} = H(s)$$

This function as itself is useful in vibration analysis; however, it can be manipulated further to provide another benefit. Because the variable *s* is a complex number, the final ratio will be in terms of both real and imaginary numbers. If only the imaginary values of *s* are considered, the function would lie solely on the imaginary axis. Plots along this axis describe the frequency of the vibration [9].

For the FRF signals used for this study, an alteration to the ratio was needed. It is preferred that this information be applicable to studies on existing road bridges. Since the excitation would be the load of an unknown traveling vehicle instead of a known impulse force, the denominator of the ratio given in Equation 3 would not be applicable. Instead, the ratio used in this study was the response signal divided by the reference signal. Both of these signals, as discussed in a later section, would be FRF signals from the same body using strain gauges.

Because these signals would initially be reading strain in the time domain, they would need to be transferred to the frequency domain using a transform function. With the previously discussed FRF calculations, the transform function was calculated using Laplace transforms. Analytical solutions that have known excitations are more easily solved using Laplace transforms [10]. For an unknown random signal, the most logical transform method, and the one used in this study, would be Fast Fourier Transform, or FFT. For this study, the FFT function in Matlab Simulink was utilized. This calculates the FFT by sampling the given data (i.e. the strain readings) at a predetermined sampling interval.

Because this preceding derivation of the FRF was simply for the general case, modifications should be made for strain data. However, the general equation for a frequency response, shown in Equation 3, is still relevant no matter how the data is acquired. An FRF can be calculated as long as two signals, both transformed into the frequency domain, are used in a ratio [11]. It is simply the output, or response, divided by the input, or reference. Several forms from a variety of transducers have been used successfully to calculate a frequency response signal, such as acceleration [6] [12] [13] [14], displacement [6] [15] [5], and strain [4] [7] [16]. The approach for this study is that the reference signal will not be an excitation, but will instead be another sensor reading. The equation for the approach, shown below in Equation 4, serves two purposes: it calculates the FRF signal and it converts the magnitude into decibels (db).

(4) $$FRF = 20Log_{10}\left(\frac{response\ strain}{reference\ strain}\right)$$

As shown in Equation 3, an FRF signal is affected by three parameters of the beam: mass, stiffness, and damping. Mass is assumed constant for small volume damage such as cracks, and the stiffness is inversely related to the amount of damage. Both of these variables are determined by the finite element program. For the damping, *c*, of the material, multiple options are available during the modeling. According to the manual for ANSYS, the finite element software used in this study, transient analysis can use two different types of damping: material damping and the proportional damping method. As shown in Equation 5, the proportional damping method has each multiplier affecting its respective matrix, which in turn is summed for the damping matrix.

(5) $$[C] = \alpha[M] + \beta[K]$$

There are restrictions for each variable in the damping equation for the software package. Alpha (α) is the mass matrix multiplier, and is rarely used [17]. Beta damping (β) can only be specified once during each load step in a transient analysis [12]. Because the damping was held constant, the proportional method was the chosen method for damping.

CHAPTER 3: NUMERICAL SIMULATION

3.1 Objective

There were several objectives for the computer simulation portion of the study, as well as secondary goals that needed to be accomplished in order to complete the objectives. The first main objective was to determine if ANSYS would be able to accurately produce vibrations of the plate at different damage states. A new way of simulating damage was used in order to more accurately depict the damage without resetting the mesh, so the method was tested to ensure validity. The second major objective was to use the working model to complete a parametric study of the plate. This study was to determine the range of effectiveness for strain gauges in dynamically detecting damage.

Secondary objectives occurred throughout the completion of the study. For example, previous studies similar to this had shown that using acceleration worked very well in determining an FRF that could detect damage [18]. Therefore, an initial goal was to prove that this method could work using vibration signals from strain sensors. Also, for the method to be completed, a reference sensor, one that would remain constant throughout the entirety of the tests, would have to be chosen.

One of the last secondary objectives was to determine if there was a pattern to the parametric range as damage increased. For example, to determine if the damage increased at a constant rate, or if it only worked for certain damage states. Computer model simulation was the best method of identifying a pattern, given that many sensors points were needed; something that would have been time-intensive in a lab setting. As previously mentioned, there are four benchmarks in the area of VBDD. The proposed method's main purpose was to use FRF signals to detect damage, so the first benchmark was inherently covered. If a pattern was identified that could categorize or explain the behavior of the parametric range, it would have been possible that both the second and

third benchmarks could have been satisfied. Also, because strain sensors were being used, the stress in the member could theoretically be calculated in future work, completing the final benchmark. Therefore, identifying a pattern in the parametric range was considered a desirable objective for this study.

3.2 Numerical Model

The plate's vibration simulation needed several iterations to reach the accuracy and signal quality that was desired. An initial model was created using shell elements (Solid-187) with the top and side dimensions being used. However, the meshing with this model allowed only one element to cover the thickness of the plate; something that could potentially produce a large inaccuracy. This is because the vibration was solely in the y-direction (the same axis as the depth). One element would not have accurately captured the bending motion being experienced by the plate.

A three dimensional model was also created in order to improve the accuracy versus the shell element model. However, as with the previous model, the meshing led to complications in the elements in the vertical y-direction. In order to create enough elements over the depth, the mesh needed to be extremely fine. Because the length was so much greater than the depth, 288 times greater, an element size that satisfied the depth consideration produced a superfluous number of elements in the longitudinal x-direction. Again, the element size in the longitudinal, and especially the horizontal z-direction, was not seen as important as the size in the y-direction. This extreme number of elements, ones that didn't improve the accuracy of the vibration, made the model very time-intensive.

The final iteration was used for two reasons; it meshed many more elements along the depth of the plate without being overly time-intensive, and it allowed the new method of damage simulation that wasn't possible in the previous two iteration styles. This final iteration modeled the depth (y) and longitudinal (x) directions using areas meshed with

Plane-183 elements. These elements were also given a real constant that provided a depth of 3 inches. After solving, to extract the strain data from the model, an element and a node were chosen. Averaging over the element, the strain at the node was given. Therefore, an element with an increased number of nodes would have increased the accuracy of the calculation. Because of this, a 10-node element was chosen.

The second and more important reason for using Plane-183 elements was to be able to simulate damage in a unique way. Previously, damage was induced by lessening the stiffness of a cross-section of the beam [18]. To model the beam, three areas were created; one for the cross-section, and one for each side of the damage. This allowed the mesh to be consistent throughout the model so that no irregularities with the elements' shape were produced. Another advantage for this method was that remeshing was not required; the elastic modulus of the cross-section could be decreased and then the solution would be solved again. Keeping a consistent mesh would mean keeping the same nodes and elements, a benefit when the strain had to be extracted from the same locations at each damage state.

However, these conveniences produced a possible inaccuracy when comparing the results to the lab plate. In the lab, the plate had a notch grooved into it using a CNC machine to a specific depth. Therefore, the grooved area had an elastic modulus of zero (due to no material), while the non-grooved area still had its original elastic modulus. The previously mentioned modeling method ignores this disparity and simply assumes that the entire cross-section has a decreased elastic modulus.

To remedy this, while still keeping the conveniences of the model, the original areas were initially modeled. The areas representing the healthy beam on the sides of the damaged cross-section were left unaltered in both dimensions and mesh size. However, the damage area was revised. For each percent decrease in damage, an area with a depth matching the same percentage of the total height was created. As shown in Table 1, these areas corresponded directly to the depth of the groove on the lab plate for each damage

state. Because the depth of the areas changed, so did the element size for the mesh. This allowed a constant number of elements for each damage area. In order to increase the damage, the elastic modulus was changed from 29,000,000 psi to 10^{-6} psi to mimic the stiffness of no material. Setting the elastic modulus of the area equal to zero would've produced non-convergence in the model. However, due to the large difference between the values, it acted as if it was equal to zero.

For this model, it was possible to just remodel the plate with the rectangular notch grooved out for each damage state. However, this method was used to show that it could work on other, more complex-shaped beams as well. With beams more complicated than the plate, remodeling may not be a practical solution. Even with the simple plate used in this study, remodeling, remeshing, and then extracting data from a new shape would have been a tedious process.

The method decided upon keeps the benefits of easily creating damage from the original method while more accurately modeling it according to the lab specimen. The only other change that was made was to gradually decrease the element size from .05 inches in the healthy areas to as little as .0025 inches in the damaged section. This produced a small number of warnings from the software due to irregular shapes of the elements. The issue was solved by using more areas, with lengths of 4 inches, located on each side of the damaged section. These areas, labeled as 'transition areas' in Figure 3, had elements with dimensions of .0125 inches. This allowed them to properly mesh with the smaller elements of the cross-section while not meshing the entire plate with such small elements, thus wasting time in solving the model. It should be noted that all areas were Boolean glued, allowing them to possess different properties and mesh sizes while also "communicating" between boundaries.

Table 1: The depths of the damage state areas. Each area-number relates to Figure 1.

Damage [%]	Depth [in]	Area #
5	0.013	1
10	0.013	2
20	0.026	3
30	0.026	4
50	0.052	5

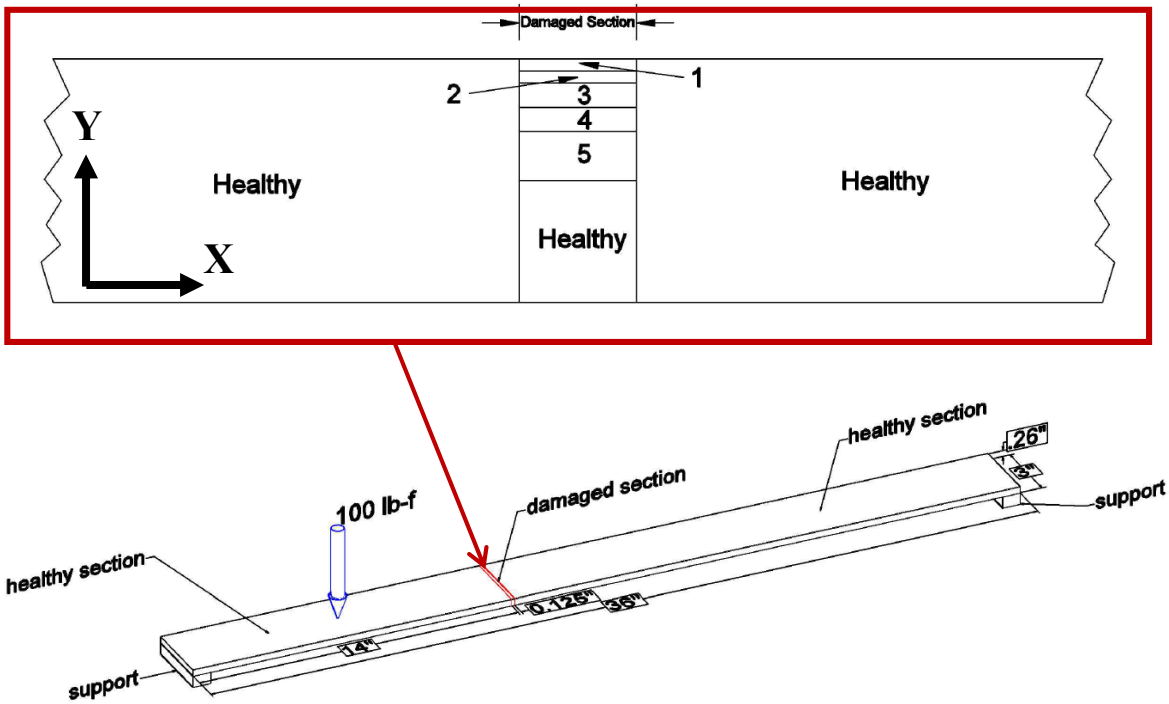

Figure 1: A zoomed-in side-view of the damaged section before meshing. The areas labeled 'Healthy' on the side view are areas never damaged. The numbered areas correspond to Table 1. Also shown is a 3-D schematic of the plate.

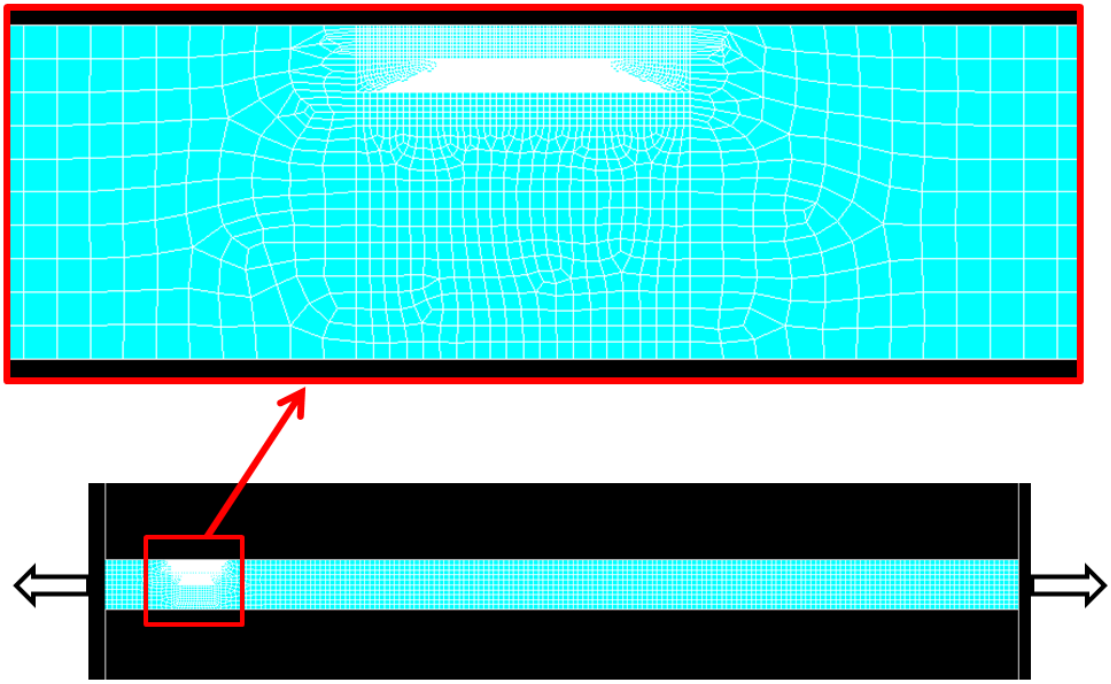

Figure 2: Side-view of a zoomed-in look at the damaged section's mesh, as well as how it transitions into the rest of the beam. For clarity, the entire beam is not shown.

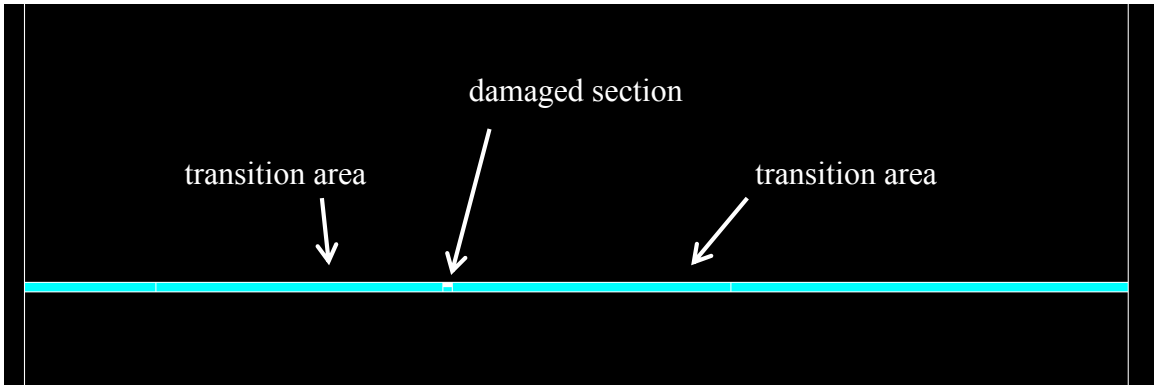

Figure 3: The areas used to create the mesh, including the damaged cross-section and the transition areas on both sides. For clarity, the entire beam is not shown.

The actual pre-processing modeling was straightforward. Because of the chosen elements, as discussed previously, areas were modeled until a large compiled area was created. This became the depth and length of the plate, with dimensions of 36 inches by

.26 inches. After all the areas were created according to the damage methodology, the mesh was applied. Using the proportional damping method, a value for beta (β) of .01 was used for all areas during the entirety of the experiment. This was based on a range of .01 to .05 given by previous research [19]. Another study used a value of .01 for their damping value and kept it unchanged throughout the experiment [5]. The mass multiplier alpha (α) was not used in damping. This method of damping, proportional damping, was chosen by the capabilities of the software. For transient analysis, ANSYS recommended using this damping method instead of constant material damping [17].

3.3 Boundary Conditions

For the boundary conditions, it was assumed that both ends were fixed. However, this did introduce the possibility of error, as is common with boundary condition assumptions. The goal of the initial simulation was to replicate the laboratory specimen. In the lab, the plate was taped down at both ends, preventing any motion; therefore, the fix-fix assumption seemed valid. To simulate this as closely as possible, the amount the plate was taped down on each end was measured in the lab. Each node on the bottom surface of the plate the same distance as the lab, a length of .75 inches on both ends, was then fixed in the x (horizontal) and y (vertical) direction. Much like the experimental setting, it prevented longitudinal and vertical motion, but it did not resist a moment. Also important was that the vertical faces of the plate ends were unrestrained, so that the top of the plate was able to strain while the bottom was held stationary.

3.4 Loading Function

To begin the tests, a dynamic study was carried out using the full-solution transient analysis option. This allowed the use of a step-function, a useful tool when replicating the load of an impact. For the loading, two load-steps were used; the initial load-step that applied the impact load and the final load-step that was used to view the vibrational response. It should be noted that the only difference between the load-steps

were the applied loads. The boundary conditions remained consistent throughout the analysis.

The first load-step occurred over a time interval of 0 to .01 seconds, with a time step of .005 seconds. At x = 7 inches, the same location for both the model and the lab plate, a ramped load of 100 lbs in the negative y-direction (vertical) was applied. The second and final load-step covered a time interval of .01 to 3 seconds, also with a time-step of .005 seconds. A time-step of .005 seconds was arbitrarily chosen as a sufficiently small interval so that the response would be depicted accurately. Each time-step, the program calculated the elemental strain. Overall, each element used to extract the strain data provided 600 points of data. If these points were graphed with respect to the length of time they were calculated, each sensor location would give a plot similar to Figure 5.

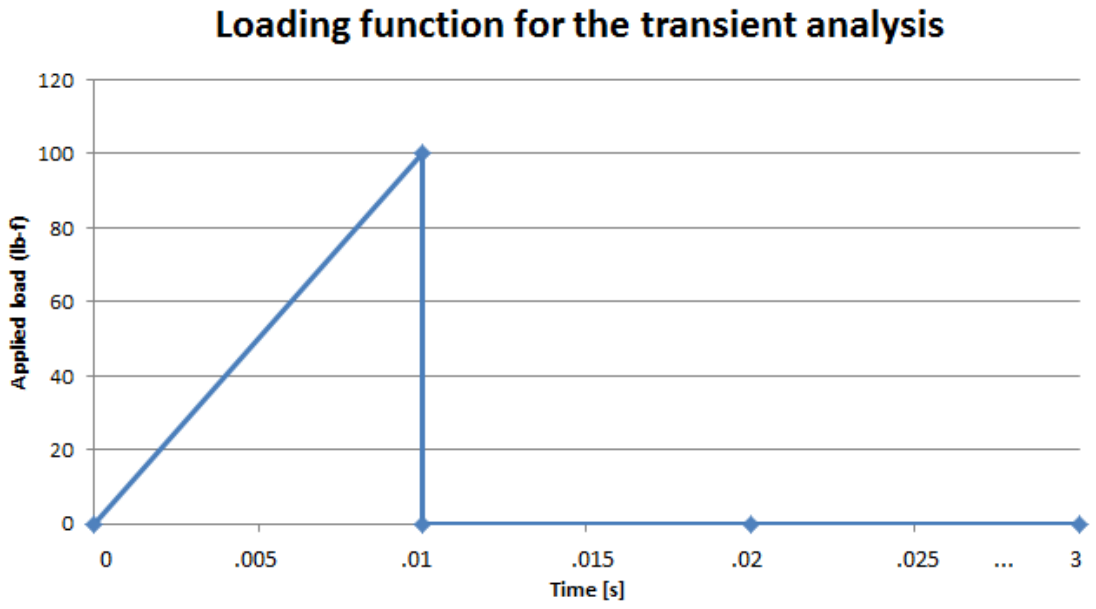

Figure 4: The ramped loading function of 100 lb-f in the negative y-direction.

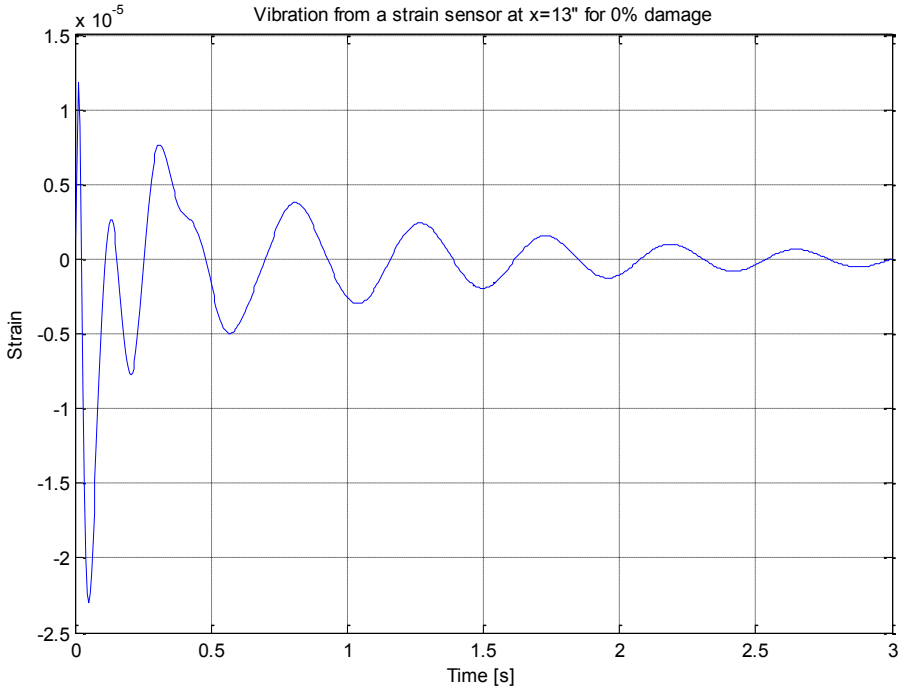

Figure 5: The strain at sensor 38 (x=13”) over a time period of 3 seconds.

The advantage of the computer model over lab experiments is that data from any location on the plate could have been analyzed. This allowed a much more accurate range to be created by calculating the strain at many intervals along the plate. For this model, a total of 86 elements (1 reference sensor and 85 response sensors) were used ranging from x=1” to x=25.5”. The reference sensor was eventually located at 26.5” from the end. The spacing between the sensors was .5” near the plate’s ends, and it decreased as the sensors approached the damage. The smallest interval used was .125”. An increase in the number of sensors near the damage was to ensure accuracy when creating the effective range.

This thesis describes the modeling portion of the study separate from the lab portion for clarity in the details; however, the two portions began simultaneously and continued in somewhat the same fashion throughout the entirety of the study. Mostly, this was to calibrate the computer model so that it produced FRF signals as similar to the lab experiments as possible. Several parameters were shifted within an accepted range until

the signals showed the same characteristics. For example, if the FRF signal from the model showed a natural frequency at a lower frequency than the lab testing, the damping ratio could have been reduced, thus making the model stiffer and producing more of the higher frequencies. Other parameters, such as the elastic modulus or Poisson's ratio, could have been altered, but only slightly. For the study, they were held constant at their accepted standard values. The elastic modulus, E, was defined as 29,000 ksi and Poisson's ratio, ν, was defined as .3.

3.5 FRF Calculation

The data from each damage state was exported from ANSYS in an 86×600 matrix using a .csv file. After converting this to a compatible matrix in Matlab, it was converted using a separate program into an FRF signal. This program used an FFT (Fast Fourier Transform) to convert the data from the time domain to the frequency domain. The magnitude of the FRF signal was displayed in decibels (db) by multiplying the vector by 20Log_{10}.

As mentioned in Chapter 1, the FRF is normally calculated by creating a ratio of the output signal to the excitation force. However, this study used two signals to create the ratio. To accomplish this, the Matlab script converted both signals to the frequency domain, then divided the response vector by the reference vector to create the ratio.

An FRF and a resulting graph were created for each ratio during both tests. For each one, the FRF graphs were plotted together from each sensor for all the damage states. This preliminary step best allowed the comparison of the outputs as the damage increased. However, graphically comparing would not have given a full comparison, so numerical integration was used to identify the magnitude of the differences.

While running the analysis, a frequency spectrum had to be chosen. If the range was too small, there was a chance that dominant frequencies were being left out; if the range was too large, high frequencies that may be noise or other non-dominant

frequencies could have affected the analysis. Therefore, it was chosen to focus on a range of 0-100Hz for the spectrum. This range could then be truncated more in the later stages of data analysis after the dominant frequencies were observed. A 100 Hz range seemed suitable given the nature of strain gauges. The types of sensors used in the lab experiments were able to only observe low frequencies, as opposed to accelerometers that are able detect a wider range.

3.6 Damage Identification

For the following discussion regarding the initial damage detection method using ANSYS, a numbering system for the sensor nodes will be used. This is outlined in Figure 6 below. The location of the sensor nodes and the applied load, shown in the figure with an empty circle, match the setup in the lab experiment. Only four sensors were used in the damage detection procedure to ensure simplicity, as well as to match the lab procedure. As shown in the figure, the sensors are numbered one through four (the reference is sensor four), moving from left to right. Later, in the parametric study, the sensors will again be numbered in ascending order moving from left to right.

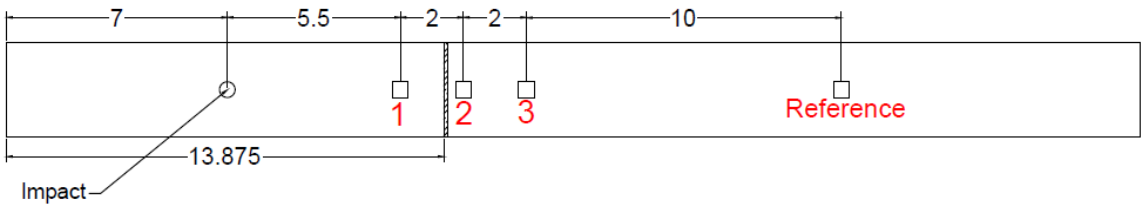

Figure 6: A top-view showing sensor nodes numbered for ease in description. The un-numbered circle is the location of the applied load. All dimensions given are in inches. The reference sensor is also referred to as sensor four.

The main objective of the first test in the simulation was to determine if damage could be detected using an FRF method from strain sensor signals. Also, a pattern needed to be detected in order to establish a way to determine the level of damage that had

occurred. Therefore, the results from each damage state were compared at each sensor location. This information also provided insight into determining the optimum reference sensor. However, all of this depended on identifying a logical pattern to the FRF output as damage increased.

Multiple comparison methods were tried in order to determine a pattern in the FRF output as the damage increased. Overall, two methods were used; graphical representation and numerical integration using Matlab's built-in Newton-Cotes trapezoidal function. Both have their advantages; graphical representation was an efficient way to show the change and identify patterns, while numerical integration more accurately and quantitatively showed the differences.

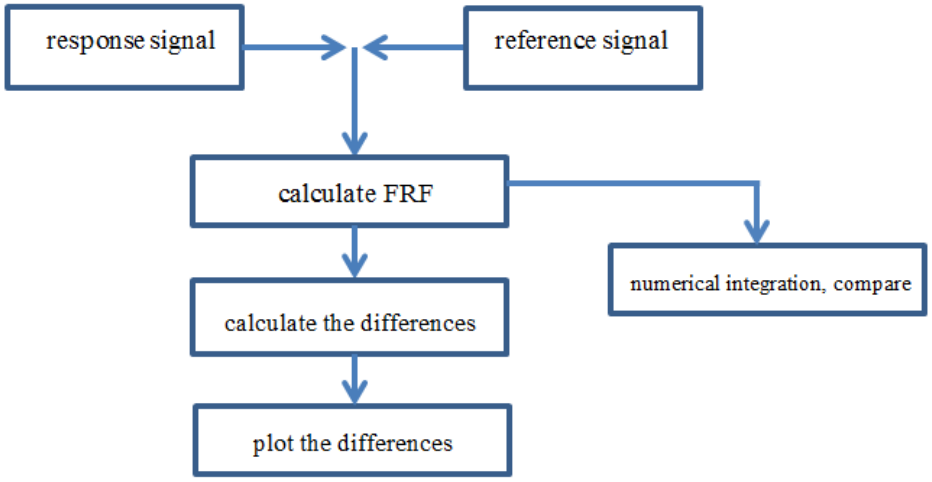

Figure 7: The process to determine if damage was able to be detected analytically.

The biggest downfall of these methods, especially the graphical, was that the difference was too small to determine an accurate pattern of change. As can be seen in Figure 8, the differences were noticeable, but were too small to easily assess. Therefore, it was decided that in order to better show the differences graphically, the differences

needed to first be calculated based on the FRF data. This allowed the scale to be magnified, and more drastically showed the differences.

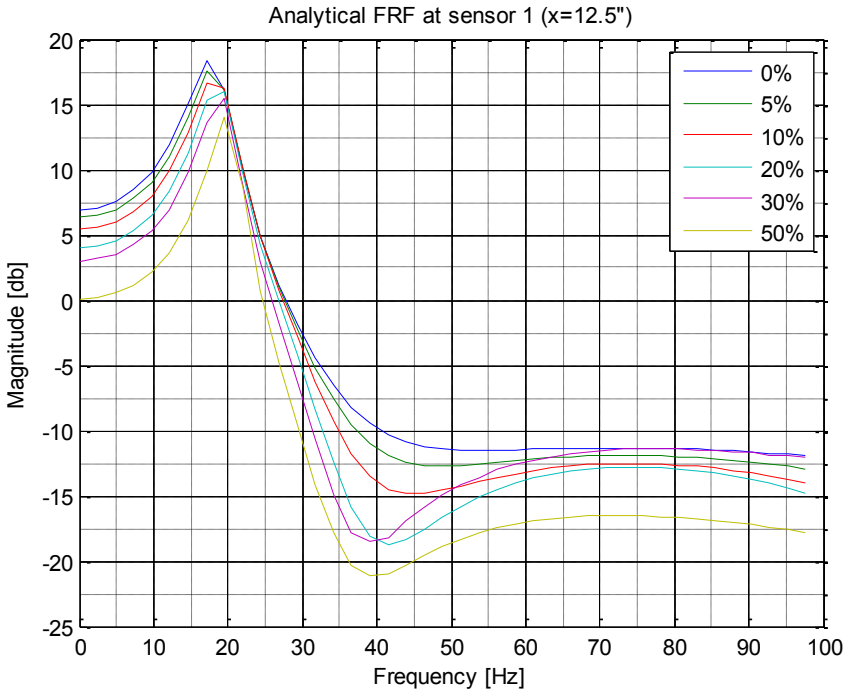

Figure 8: The FRF outputs using the ratio between sensors at x=12.5" (sensor 1). Each damage state is shown.

For the difference plots, the natural frequencies were still visible. The data for the dependent variable was created by subtracting the FRF data of a sensor at a damaged state from the FRF data of the same sensor at the healthy (0% damage) state. This simple subtraction showed how much the FRF output would change as damage increased. No other manipulation was performed.

There are several interesting points to note about a difference graph. Using Figure 9 as an example, there was a large difference slightly to the left of the peak on the FRF graph. This indicated that there was a small frequency shift between the damage states. As mentioned previously, it seems that a difference graph exaggerated the

difference between damage states. This property could be useful in damage detection. However, the magnitude of the difference is not linearly related to the percentage of damage incurred on the plate. Nevertheless, even damage at 5% shows a difference in the FRF output.

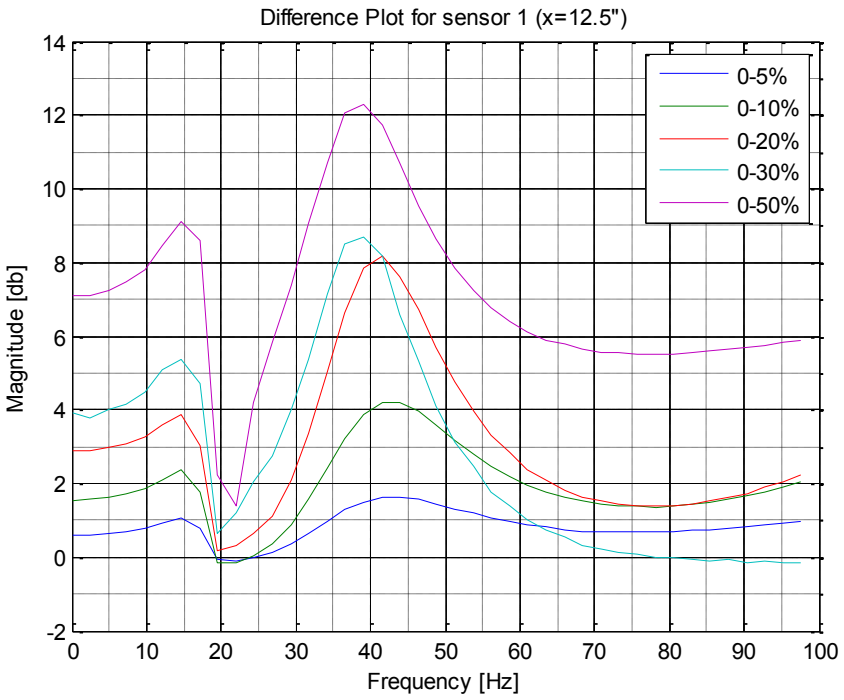

Figure 9: A plot of the differences using the healthy state as a baseline. All plots on this graph are derived from the ratio using sensor 4 as the reference and sensor 1 as the response.

Another point to take away from this test was the determination of the best sensor to use as the reference. Each sensor was used as the reference, with the other three then being used as response sensors. After comparing the FRF plots and the difference graphs for the four reference possibilities, it was found that the sensor farthest from the damage was the best choice. This could be due to the sensor not being affected by the change in vibration caused by the damage. The chosen reference did not experience any noticeable

change in strain between damage states. Creating a neutral basis of comparison such as this allowed the change in other sensors to be more clearly shown. For the remaining tests discussed in this paper, both analytical and experimental, the sensor located at x=26.5" is used as the reference sensor. A portion of the graphs used to determine the reference sensor, Figure 24 and Figure 25, are shown later in Chapter 5.

The other method used to compare the damage states was numerical integration. This method, because it was more quantitative than the difference method, was more useful to compare the data. It was able to break down the data to single values that could be plotted with bar graphs so that a trend between damage states would become clear. Later in the study, while performing the parametric tests, the numerical integration method again became critical. Also, this method served another purpose: it was the best way to compare the FRF signals from the computer model to the lab plate. The bar graphs containing the six values from each damage state, representing the three FRF results from the four sensors, should be similar to the three bar graphs produced by the lab experiments.

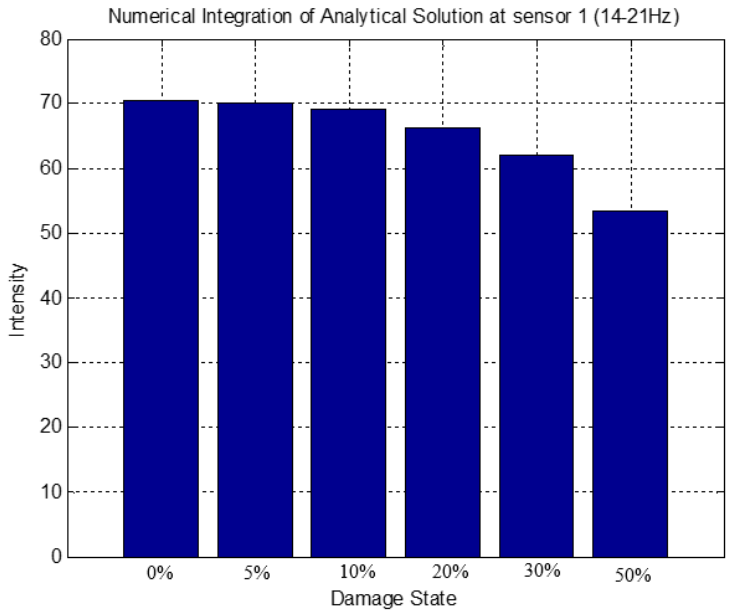

Figure 10: The numerical integration method at sensor 1

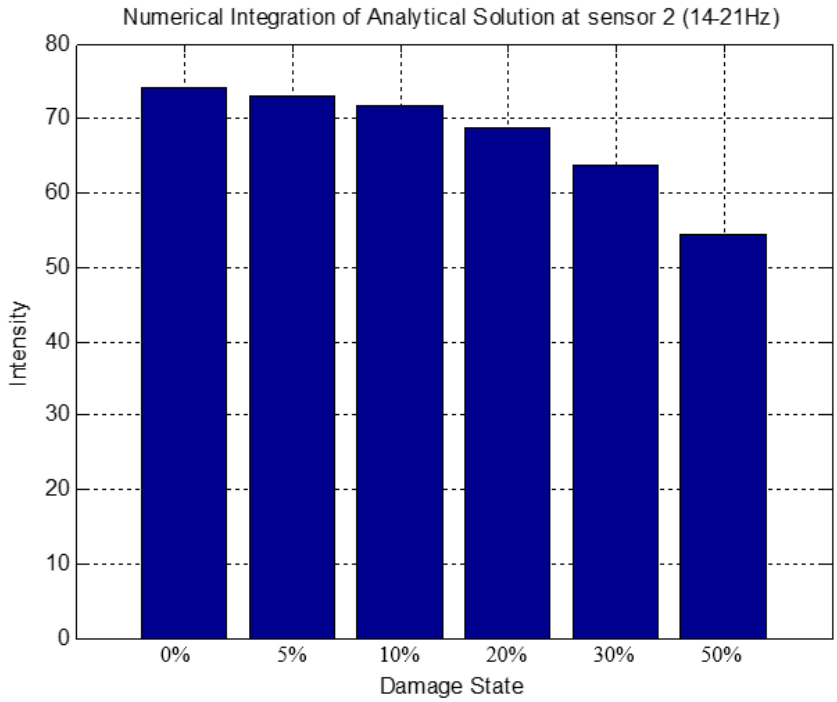

Figure 11: The numerical integration method at sensor 2.

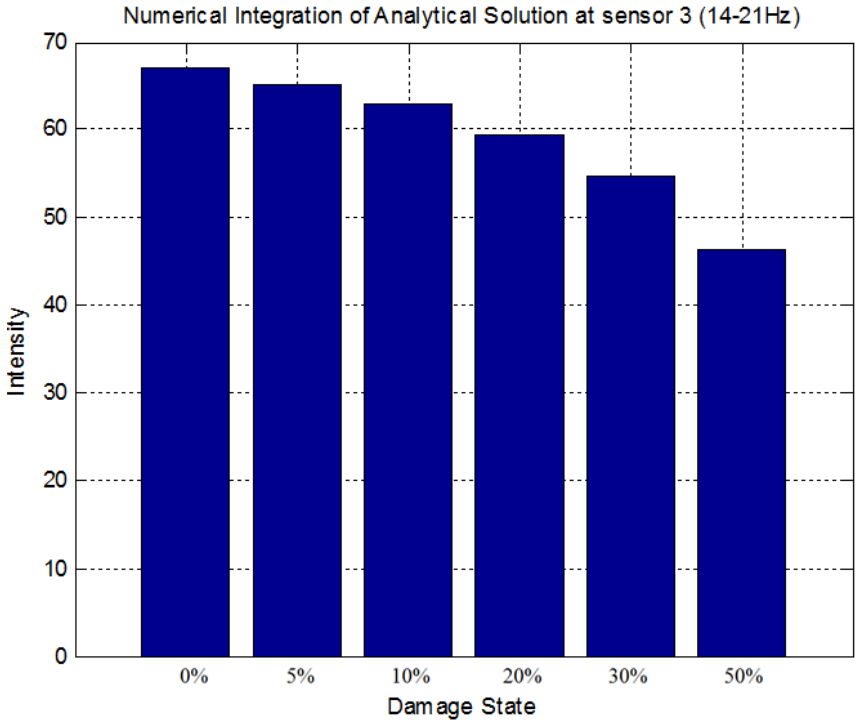

Figure 12: The numerical integration method at sensor 3.

3.7 Parametric Study

After it was shown that the method could be used to identify damage in the plate, the next objective in the study was to identify an effective range away from the damaged area for damage detection. Outside of this range, and the difference in FRF signals would have been too small or erratic to reliably detect damage. Disruptions in the range, or sections in the range where the method would be invalid, would also need to be found. Secondary objectives included identifying a pattern to the range between the damage states, and also constructing a repeatable method in order to get the range for other specimens.

Much like the previous test of simply detecting damage in the finite element model, this test extracted strain from certain sensor nodes at each time step. However, the number of these sensors increased to a total of 86, with one reference sensor and 85 response sensors, shown below in Figure 13. As was mentioned before, the number of sensors increased as the location approached the damage area, shown with the hatching. With the plate 36 inches in length, the first response sensor, starting from the left, was located at x=1" and the final response sensor was located at x=25.25". For further reference in this study, these sensors will be numbered from left to right in ascending order. A complete list of each sensor's position is given in the appendix.

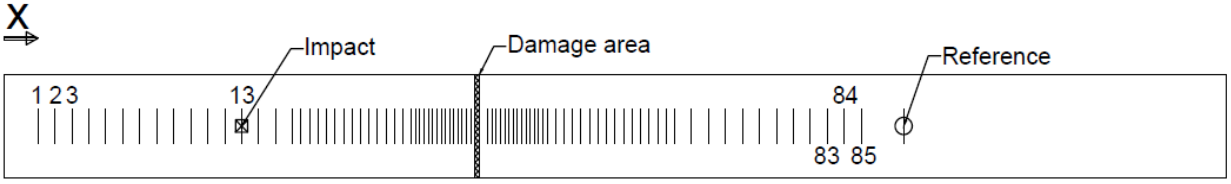

Figure 13: A top-view showing the location of the sensor nodes from the parametric study conducted in ANSYS. The response sensors are simple dashes, and the reference sensor is the circle with a dash through it. Sensors 1, 2, 3, 84, 85, and 86 are shown for clarity. The damage area lies between sensor 44 and sensor 45.

A repeatable method is important because the process should be able to be used on any structural member. Although this study does not cover strain in a three-dimensional situation, it would still be relevant on a longitudinal two-dimensional case. Therefore, a simple algorithm was developed that could be used on any large set of transient strain data.

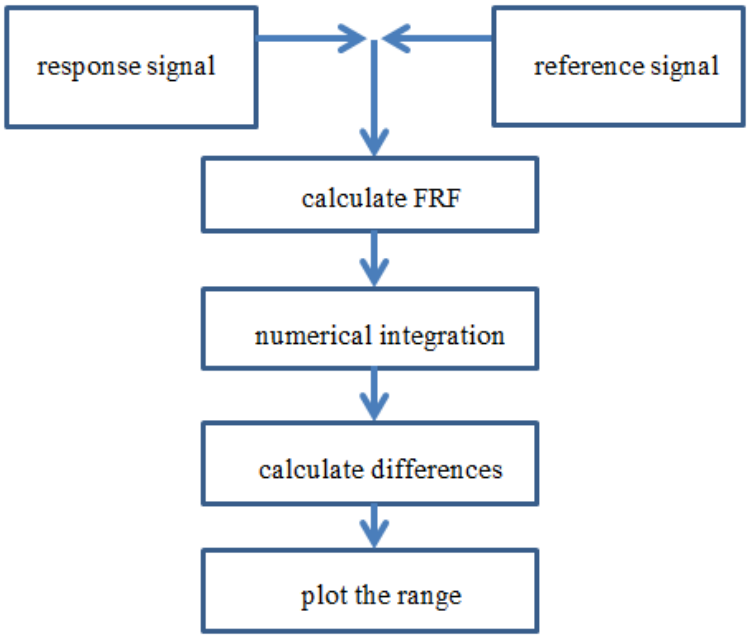

Figure 14: An algorithm for identifying the useful range of FRF signals.

The parametric study used the same type of data as the damage identification test, so no new adjustments were needed with the ANSYS model. All the initial steps for the modeling and data analysis were the same for both tests. However, the process diverted after the FRF signals were calculated.

For the parametric study, one of the initial difficulties was finding a way to compare several different variables at one time. For example, the FRF signal for each sensor needed to be compared for all damage states. Because the FRF signal was a

column vector of data, thus having two dimensions, it created too many dimensions for a proper comparison. Overall, there were four variables to factor in: the strain sensor location, the frequency of the FRF, the magnitude of the FRF, and the damage state. A solution to this problem was needed that still accounted for the behavior of the FRF at each sensor location. The change in the FRF needed to be tracked at each sensor on the plate, which would allow the change over the length of the plate to be viewed.

The solution to this was to reduce to the number of variables from four to three by using numerical integration. By calculating the area, the method used only one variable to account for each FRF plot. This single value, or intensity, still kept the important aspect of the FRF so that it could be compared to other damage states. Numerical integration also had the benefit of factoring in both the amplitude of the FRF signal and any frequency shifts that were present.

In order to keep the true meaning of the intensity of the FRF signal, the data was truncated down to focus on only the natural frequency's peak; 16 to 24 Hz. This allowed the integral to only measure the data around the natural frequency. Without this truncation, the values and then the range plot could be distorted. Also, the natural frequency provided a large difference between damage states, it had a consistently high coherence between the signals, and it expanded on the process of tracking the amplitude of the perceived natural frequencies [4] [5]. The numerical integration was computed using the Newton-Cotes trapezoidal function, "trapz," provided as part of the Matlab toolbox. Before the integration started, the accuracy of trapz was tested using a known oscillation function. Comparing the exact solution of the integration to the solution using the trapz function, the error was less than .05%.

After the numerical integration, each FRF signal for each damage state was represented using a real number value. Another step after this was needed for the plotted values to show change. Each damage state needed to be compared to the healthy state in order to be able to identify a relationship to the other damage states as damage increased.

To show the change, the difference was calculated for the value of each sensor from the healthy state to the given damage state. This approach was similar to calculating the differences during the damage identification test discussed in the previous sections. However, it should be noted that the two plots have two separate interpretations. The difference for damage identification was the difference between the values of a single FRF for the damage states; the sensor location was constant for each plot. For the parametric study, the difference was between two entire FRF intensities, so both the location change and damage change can be shown on the same graph. This difference calculation provided five vectors with 85 columns that were plotted simultaneously. Each column represented the difference between the healthy state's intensity and the damage state's intensity along the length of the plate. There were five vectors to represent the difference between each damage state, and 85 columns because each column represented a location where data was extracted to calculate an FRF signal. To better understand the plot, a list of each sensor's location is given in the appendix. Pertinent locations are provided on the graph.

Other methods were tried that did not achieve as decisive of a range as the plot shown in Figure 15. One example skipped the step of the numerical integration. Instead, to reduce the variables from four to three, the total difference between the healthy FRF vector and the damage state's FRF vector was summed for each sensor. It was then plotted in a similar way to the graph in Figure 15. Two other methods that were tried involved adjusting the FRF signal before using numerical integration. The first was to determine the absolute value of each value in the FRF vectors for every sensor. A graph of an FRF with this approach would have an unaltered positive section and the mirror image of the negative section. The other approach was to adjust the FRF vectors so that the minimum value was zero. This was done simply by adding every term by the absolute value of the largest negative term. All of these approaches were completed with the data in order to find the best way to determine a range. However, these approaches showed

little to no relationship between damage states and the location of the strain sensor to the damage.

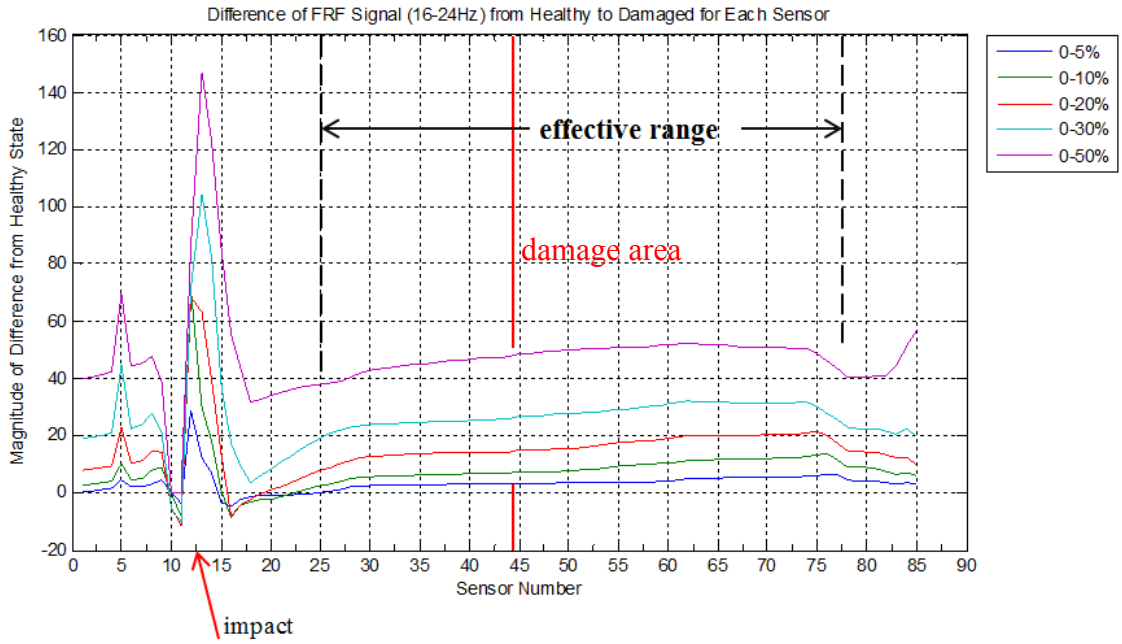

Figure 15: The plot of the FRF differences used to identify the useful range.

Previous research has used only the amplitude to compare the strain FRF signals between damage states [5]. This method was used and it yielded very similar results to that which is shown in Figure 15. However, this study used a truncated range by way of numerical integration in order to factor in the frequency shift of the signals. This frequency shift did not play a large role in the differences between the signals.

CHAPTER 4: EXPERIMENTAL STUDY

4.1 Objective

The main objective for completing the experiments on a simple plate in the laboratory setting was to validate the findings from the finite element procedures. If the plate responded similarly using both finite element models and physical experiments, it could be assumed that the parametric study using FEA would also be relevant in a realistic setting. This allowed the dexterity of the computer model without having to apply innumerable strain gauges to the plate in the lab setting. Conducting a parametric study on the lab plate was not an objective for this study due to the present limitations and the general infeasibility of the procedure. It wouldn't have been practical to attach 86 strain gauges to the plate for two reasons; the time it would have taken to adhere the sensors and the space requirement for one sensor. It was much more practical to simply validate the computer model with the lab plate.

4.2 Initial Plate Setup

A plate was chosen with the dimensions of 36in. x 3in. x 1/4in made from A-36 structural steel. Although the shape isn't applicable to realistic settings, the material properties and frequency responses due to vibration are similar to what could be encountered in real-life applications. Therefore, the results from our model could be applied to other structural members. All tests were conducted on a stationary shaker table with an isolated foundation to eliminate the ambient vibration. The plate was affixed to the table using double-sided tape and rubber blocks with .75 inches on each end supported. These were used to further reduce ambient noise. Early in the research, it was shown that outside noise affected the signal too much when it was not on an isolated foundation. Also, in order to ensure more accuracy, for the lab tests and the computer

model, measurements of the width and thickness were taken every two inches. The data was averaged, and the plate was found to be .256 inches deep and 3.01 inches wide.

The strain gauge chosen for the experiments was a general purpose uniaxial foil model manufactured by Vishay Precision Group. A strain gauge's type matters because each type has a different sensitivity and accuracy. The measure of this sensitivity for a strain gauge is a unitless variable, referred to as the gauge factor, used in the calibration of the data-acquisition system. For example, a typical foil strain gauge has a factor of approximately 2. Semiconductor gauges tend to have gauge factors 20 to 100 times greater than that of foil gauges [6]. However, this factor tends to be less known for the semiconductor gauges than for foil gauges. Other disadvantages for semiconductor gauges include higher cost, a more involved installation process, and higher fragility [20]. Therefore, a compromise between accuracy and feasibility was made, and foil gauges were chosen.

Both strain gauges and accelerometers were attached to the plate at specific locations, shown in Figure 16 below. The location of the damage was chosen to be around the middle of the plate in order to avoid any interactions with the supports. With the location chosen, the damage area and impact zone were marked. A wide range of distances from the damage was needed, so sensors were placed between less than .5" to over one foot from the damage. This would help in determining how far away damage could be detected. Based on the findings from the analytical damage-detection model previously mentioned, the reference node was taken to be the far-right node at x=26.5 inches. The overall number of strain gauges used was limited by the number of available gauges. For clarity in the following discussion, the numbering of the strain gauges will be the same as shown in Figure 16. Each sensor will be numbered one through five in ascending order, starting from the farthest left sensor.

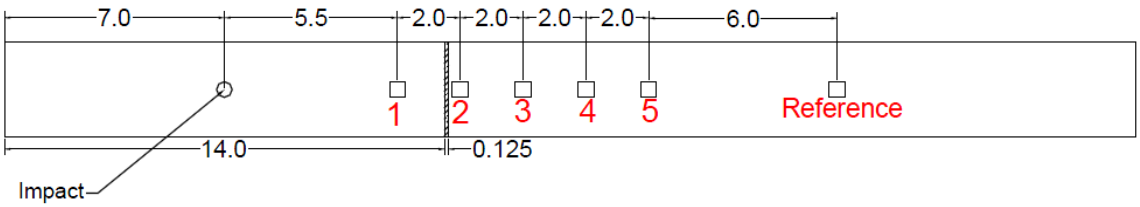

Figure 16: A top-view of the plate used in the lab experiments. Squares designate the locations of the strain gauges and accelerometers. The circle (7" from the left edge) signifies the impact location. The damage is shown as the hatched area. The units are inches.

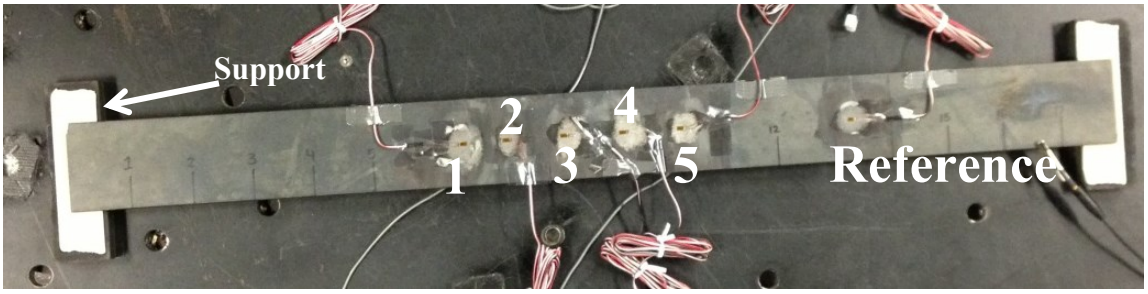

Figure 17: Photograph of the plate with the strain gauges before the accelerometers were attached. The wires attach to the DEWEsoft data acquisition system. The sensors with the corresponding numbering system are shown.

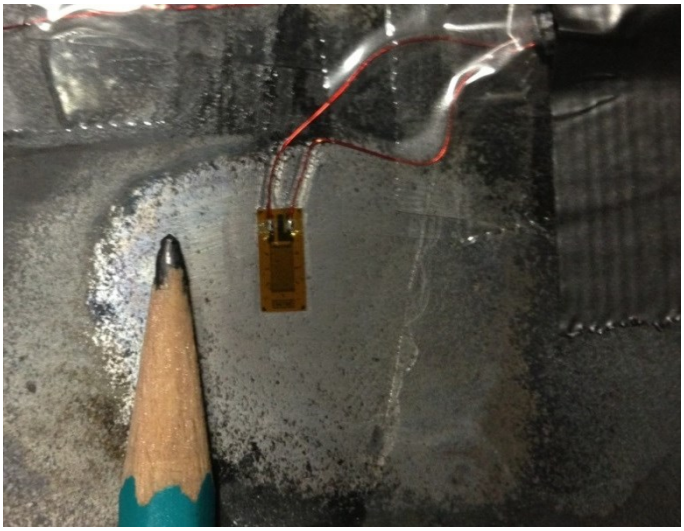

Figure 18: Example of an attached strain gauge used in the lab setup. The pencil roughly shows the size of the gauges. The tape in the photo is used to hold the connecting wires in place so they are not ripped from the gauge.

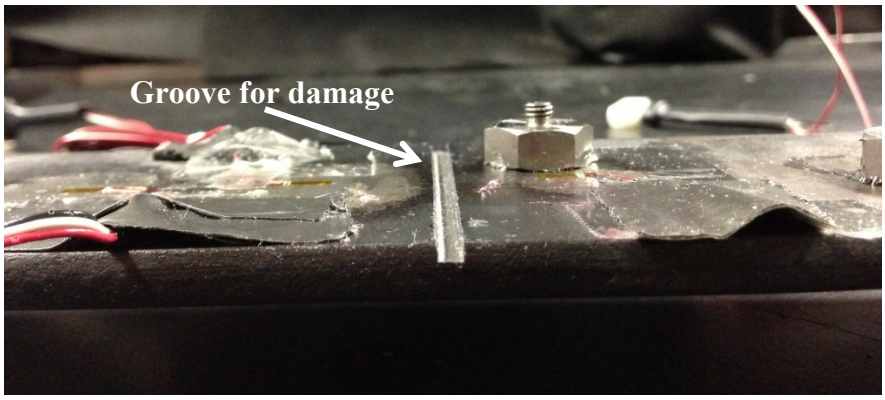

Figure 19: A side-view of the groove used to simulate damage. This was the 30% damage state. The metal hexagon glued to the plate is one of the bases for the accelerometers.

After the hardware was attached to the plate, the connections were linked, via a DEWESoft DEWE-43 data-acquisition system, to the computer. Four compatible adaptors were available with the DEWE-43, which ended up being the limiting factor in the number of gauges being used in each test. Four adaptors were also available for the accelerometers. Because of the limited number of strain gauges available, sensors one, two, three, and the reference were used. As can be seen in Figure 17 on the far right, an alligator clip ran from the data-input box to the plate to provide grounding in another attempt to reduce noise. The data acquisition system coordinated with DEWESoft software on the PC, which collected and exported the impact data.

As can be noticed by inspecting the data from sensor 2, the strain gauge was inadvertently detached before tests for the 20% and 30% damage states could be completed. This occurred after the 10% damage tests were conducted, so no data for that test was affected. Therefore, data for the second sensor from the left, sensor 2, was not available for two of the five damage states.

4.3 Procedure

One of the objectives of the lab experiments was to validate the initial findings from the finite element model, so the exact same procedure needed to be completed. This

involved identifying if strain monitoring was a viable way to detect damage in a plate using an FRF signal. Past research studies had proven that it could [21], but it needed to be shown that the setup with the chosen strain gauges would work properly. A procedure, shown in Figure 20 below, was identified before testing began. This allowed consistent results to show that strain gauges could detect vibrations well enough to identify damage in a plate, the other objective for these tests. The FRF output also showed the different comparisons of damage sensing at each response gauge; an important role in determining if VBDD was available experimentally.

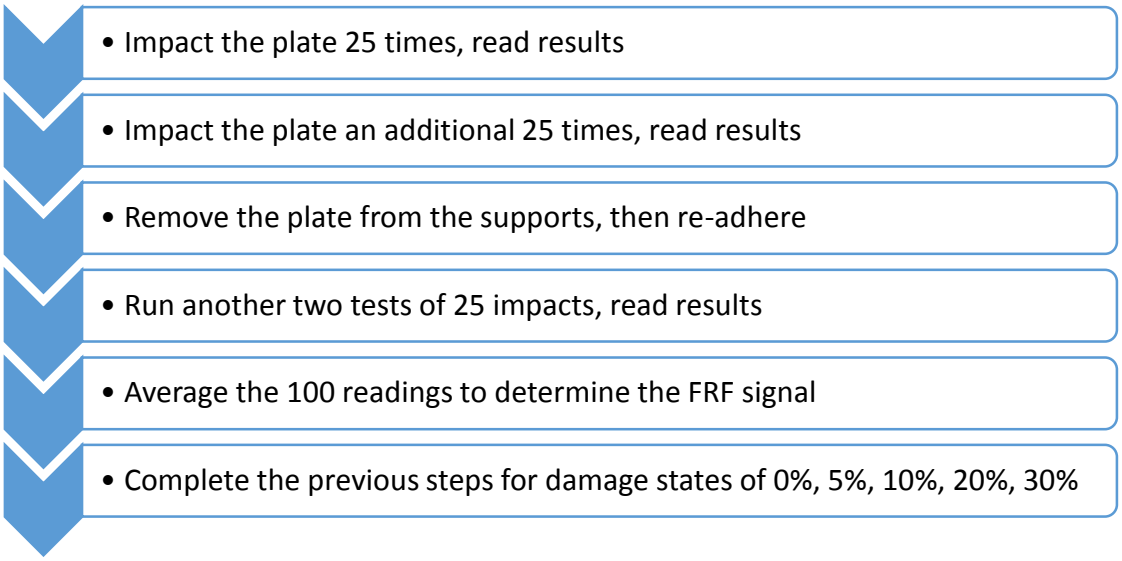

Figure 20: The procedure identified before testing began in order to produce consistent results that showed that strain gauges were able to detect damage using an FRF output.

After the plate was set as previously described, multiple tests were completed for the 0% damage state, including on several different days. This initial damage state was crucial in that it provided a baseline for comparison to the other states. Accelerometers were also used to identify the vibrational response of the plate during the healthy state. Though the FRF would appear different, the general shape and dominant frequencies

should be similar. This lent credibility to the noise-prone strain gauges after the FRF output from the two sensors showed the same characteristics. All 100 impacts occurred for the tests at the same location, located 7 inches from the left end and 1.5 inches from the top and bottom (in reference to a top-view). Damage identification should not be dependent on the location or strength of the impact; however, an impact too close to the gauge would have produced unwarranted noise.

As mentioned before, tests with this system were completed over multiple days in order to ensure that removing and replacing the plate did not affect the results, which did not occur. Another consideration taken to ensure repeatability was to remove the plate from the supports after 50 impacts, then replace the plate in the same position. Again, this was to test if the boundary conditions would change after removal. Because the plate would be removed to be damaged, it was important to make sure that nothing changed each time it was taken off the supports. Similar FRF outputs showed that no changed occurred.

After a steady image of the response for the healthy plate was established, a small groove was machined in the location shown in Figure 16. This was done using a CNC mill, so that the entire damaged area was known and there was no unknown cracks or damage that could affect further results. Using a caliper again, the damage was measured to be .127 inches wide. The depths of the groove corresponded to the percentage of damage intended. For example, 5% damage was a groove 5% of the total height, or .013 inches deep. A damage state of 10% was an additional .013 inches for a total of .026 inches. This continued until all damage states were covered. These depths match the height of each area in the damaged cross-section of the computer model.

After the data was extracted, it was run through the same programs in Matlab that were used for the analytical data. However, a parametric range, such as one shown in Figure 15, could not be completed due to the small number of data points. Therefore, a

bar graph for each sensor was created for the end result to be used for validation of the model.

In this Matlab analysis, the high number of repetitions became useful in approving the accuracy of the signal. It would not remove any noise, but the large sample produced a clear average. For each of the four 25-impact files produced during every damage state, 25 FRF signals were calculated. After determining all 100 signals, they were averaged to produce one signal that could be used for comparison. No filters were used in the analysis to smooth the signals.

4.4 Experimental Results

The main conflict encountered while collecting data experimentally was the distortion caused by noise in the system. One solution would have been to use a semiconductor gauge instead of a foil gauge. Other than replacing the gauges, several measures were taken in order to reduce noise. The most relevant was using a platform that had a separate foundation from the rest of the building. This eliminated vibration from doors shutting, people walking, and even vibrations outside the building. Further measures were taken to reduce ambient noise by using rubber blocks for supports. Finally, a grounding wire was attached from the DEWE-43 to the plate.

Even with this, noise was still present in the system. As was expected based on previous research [16], the strain gauges exhibited more noise in the higher frequencies of the viewable spectrum. This is most noticeable after 30Hz for sensor 1, 40Hz for sensor 2, and 50Hz for sensor 3. Based on this pattern, there will be less noise in the signal as the response sensor moves closer to the reference sensor.

Even with the constant issue of noise, the main objective for the experimental tests was completed: validation of the analytical data. This was met using both the general shape of the FRF signals and the relationships they shared. A general shape was important because it established the dominant natural frequency between both tests.

Mostly, this was determined by the correct estimate of the damping variables for the analytical solution. The other two variables that have an effect on the FRF, the mass and the stiffness, weren't likely to vary due to steel's constant density and elastic modulus. The peaks for all three sensors were located at approximately 20Hz, the same frequency as the analytical solution. To check the accuracy of the strain gauges, accelerometers were also placed on the plate immediately adjacent to each strain gauge. The purpose of these was to check the natural frequency; the accelerometers also showed a peak at 20Hz.

The other way the two tests were validated, and the most critical, was identifying the relationship of the different damage state signals at each sensor location. It was expected that the data would behave similar to the analytical data and decrease in magnitude as damage increased. This behavior was also shared with previous studies that identified damage experimentally [4] [16]. As can be seen in the figures below, the amplitude of the signals for each sensor decreases as damage increases. The difference in the amount of decrease is most likely due to error induced by the noise in the system. The decrease was not only shown with the amplitudes, but also with numerical integration and bar graphs.

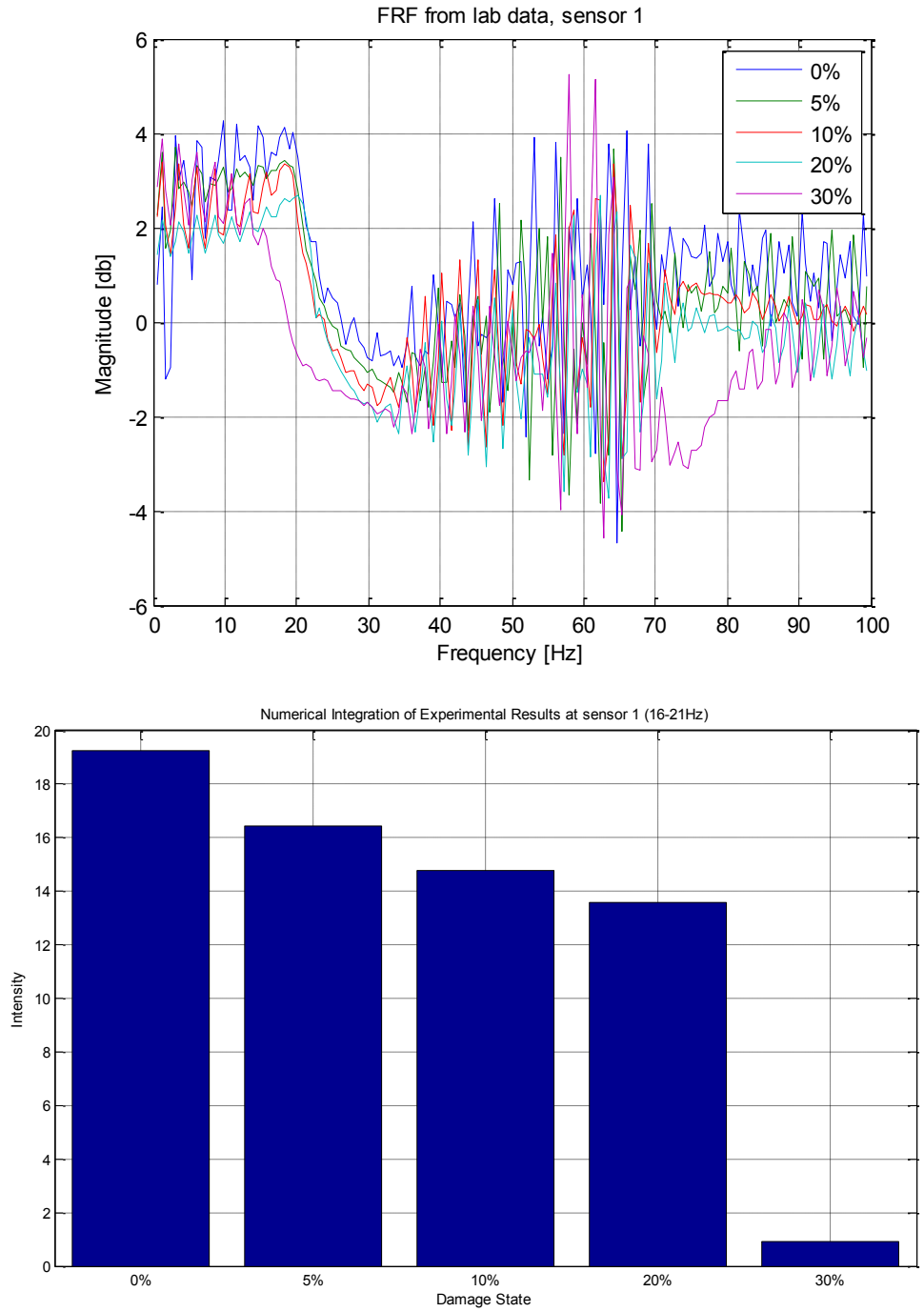

Figure 21: FRF and related bar graph of each damage state for the lab data at sensor 1.

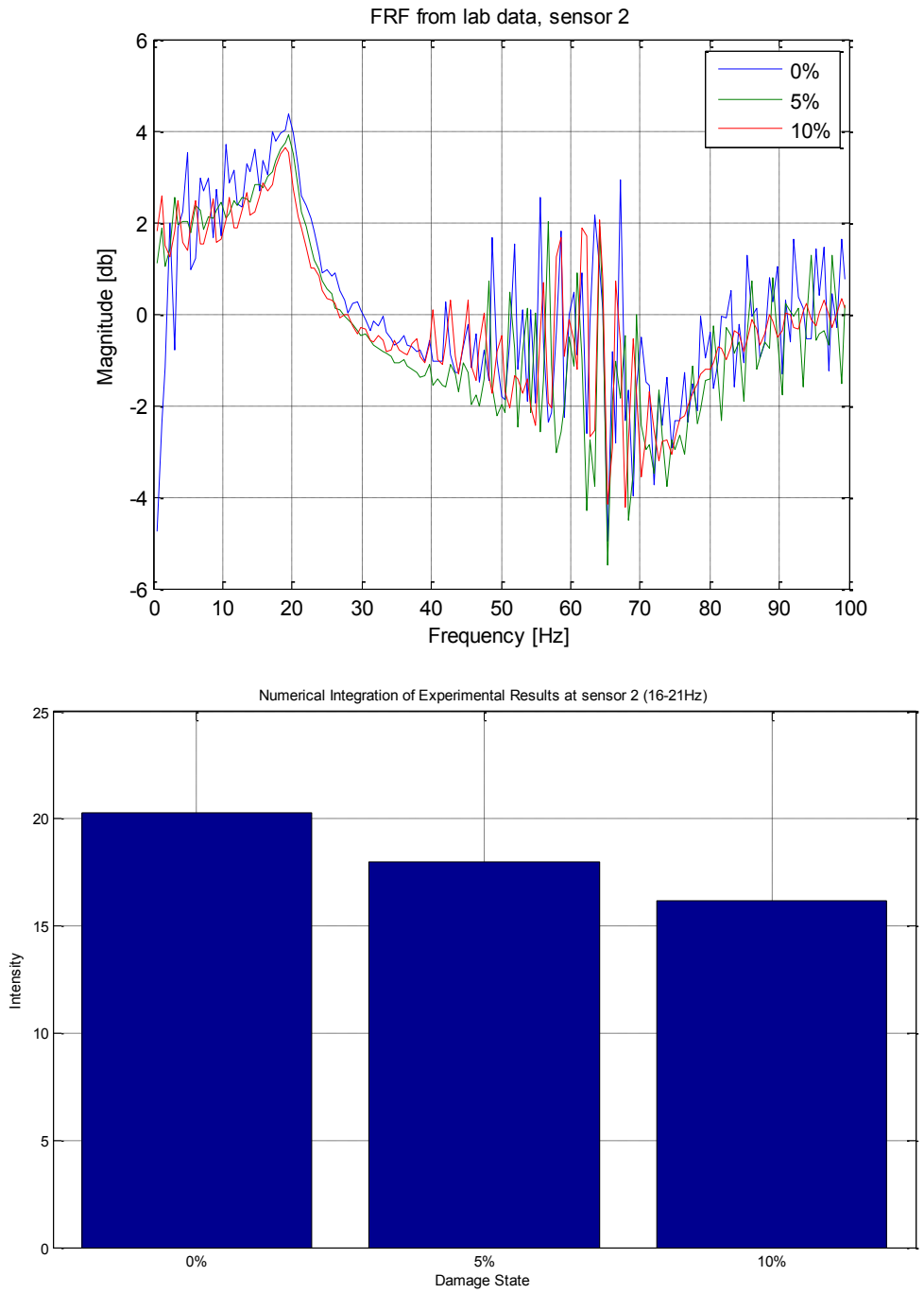

Figure 22: FRF and related bar graph of each damage state for the lab data at sensor 2. There are no 20% or 30% damage states due to the sensor's lead wires becoming detached.

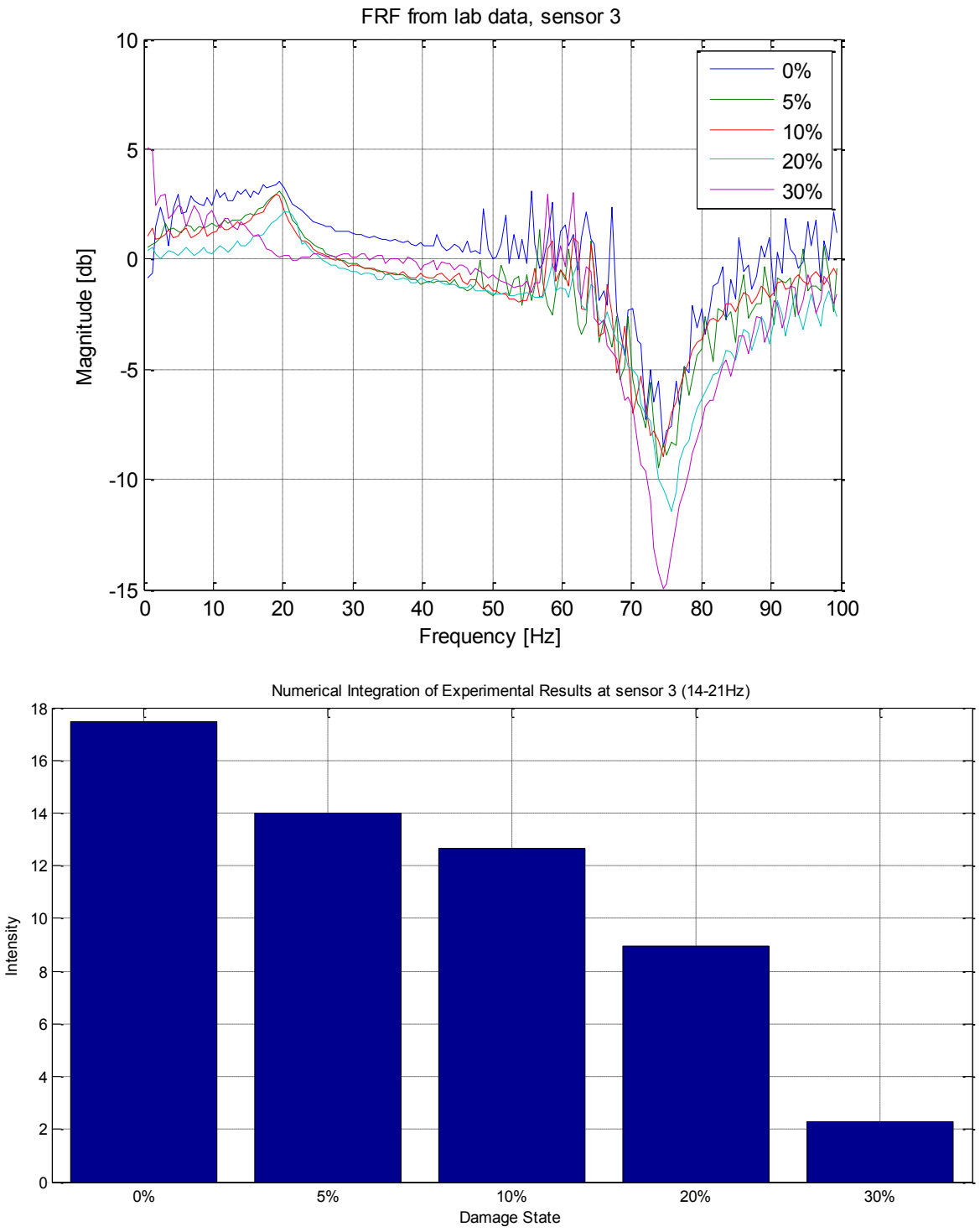

Figure 23: FRF and related bar graph of each damage state for the lab data at sensor 3.

CHAPTER 5: DISCUSSION AND CONCLUSION

Several methods used in this study could be considered novel approaches to the research of VBDD using strain gauges, but the use of numerical integration in the analysis would be most useful with future studies' data. As mentioned before, a method was needed to compress that data so that both the location and the sensor's SFRF signal could be compared simultaneously. The use of the numerical integration was found to fit this need much better than other methods.

Other methods available included comparing the difference of the highest amplitude of the signals and comparing the total differences between the two signals. Comparing the total difference was the least exact because it factored in the entire frequency spectrum. Especially with strain gauges, there could be sections of the signal that are too over-dominated with noise to be useful. Because of this, not much effort was spent using this method. The other method, comparing the amplitudes, had been used in previous studies [5]. However, the numerical integration uses the premise of this method and expands on it. Comparing the amplitudes is based on the theory that damage will dampen the signal, thus decreasing its amplitude. Therefore, the more damage there is, the farther away the peak of the natural frequency will be from the peak of the healthy state. The numerical integration expands on this by trying to identify if any frequency shifts had occurred. If the range of the numerical integration is focused on a small spectrum around the natural frequency of the healthy state, maybe $\pm$2.5Hz, then the damage state with the greatest amplitude should still have the greatest area. However, any frequency shifts would decrease the focused area of the damage states. This process would allow both amplitude changes and frequency shifts of the signals, the two signs of increased damage, to identify damage. However, it should be noted that it is important for the entire range used in numerical integration to have a high coherence between the reference and response signals.

5.1 Analytical Damage Detection

The result of the initial study was as expected; an ANSYS model was able to calculate vibrations using longitudinal strain that then showed incremental damage in the plate. This was significant because it allowed the study to proceed to identifying the working range of this method, which was the main objective. It also provided a way to validate the further analytical studies, via bar graphs, by relating them to the data found in the lab experiments. Also, by showing the basic shape of the FRF signals, and indicating that the natural frequency was at 20Hz, it gave multiple characteristics that could be compared between settings. As expected, the damage increased the damping in the model, which in turn decreased the amplitude of the FRF signals. This was seen in previous research as well [5].

The other major contribution from this simple analytical test was finding the best reference node to use for calculating FRF signals. The reference node is best located where its vibrations are unlikely to change due to damage while still experiencing similar vibrations to the response nodes during a healthy state. This knowledge was applied to both the proceeding parametric study and the lab experiments. All FRF ratios during the parametric and experimental phases used this finding and located the reference sensor at x=26.5 inches.

Choosing the reference node was based on comparing the analytical and experimental data at 0% damage. For example, by comparing Figure 24 with Figure 25, it can be seen that the data is not similar in any way. The lab data shown is for only one response sensor, but the same dissimilarity was present in the other combinations as well. When the same procedure was repeated using sensor 4 as the reference, the FRF's matched as detailed previously. Therefore, the sensor 4 was chosen as the reference for the remaining tests.

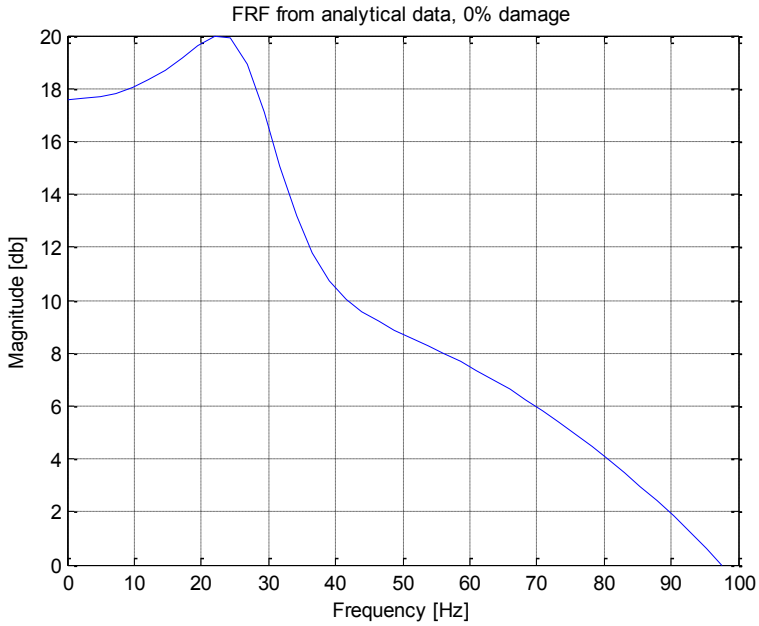

Figure 24: FRF of analytical data with sensor 1 as the reference and sensor 4 as the response. There is 0% damage present.

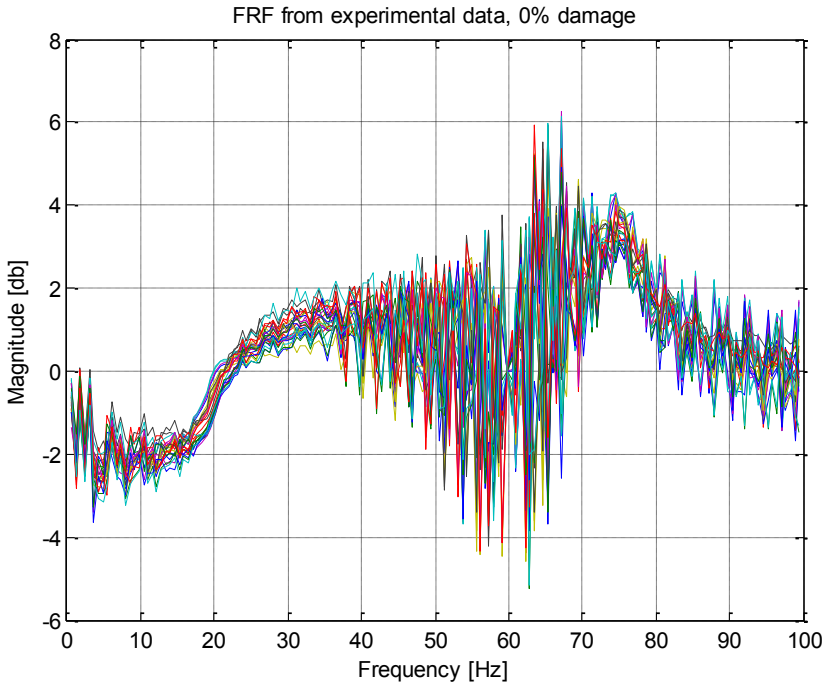

Figure 25: FRF of lab data with sensor 1 as the reference and sensor 4 as the response. This test occurred with a healthy plate. Also, FRF's from the 25 impacts of one experiment are shown.

5.2 Analytical Parametric Study

There are several important points to discuss about the graph used to identify the useful range of the strain sensors. These include, but are not limited to, the disruption of the impact, the exaggeration of the difference between the damage states, and the actual range that should be identified as effective.

There is a large spike towards the left side of the plate, and the location of this relates directly to the location of the impact; the highest point of each peak is at x=7". This disturbance is due to the erratic frequencies that come from a nearby impact. Outside of a fraction of an inch on each side, the signal returns to the normal height. Also, the left end exhibited an increase in frequency, or spikes. This is most likely due to the boundary conditions given, and the decrease in strain as the sensor location moves towards to the constrained nodes.

The amount of difference between the damage states is another important aspect of the range. As mentioned before, the difference between the healthy state and a specific damage state does not increase linearly. They do, however, exhibit the same shapes as the damage state increases. For example, in the range between sensor 18 and sensor 28, the 20%, 30%, and 50% damage state exhibit the same rate of increase in the difference. They also all have the same rate of decrease in their differences around sensor 76.

The most important objective met by this analysis was the identification of an effective range of damage detection for each state of damage. Based on Figure 15, five of the six damage states show a noticeable difference from the healthy state. The only state that would be hard to identify damage for would be 5% damage, because it differentiates noticeably from the healthy state only at the area of impact. For realistic testing, when the impact area wouldn't be a specific location, or if the impact is occurring at multiple points, identifying an impact area would no longer be applicable. For a noticeable difference on all the other damage states, the effective range would be from approximately sensor 25 to sensor 75. In the distance from the end of the plate, this

would be x=10.75” to x=19.5”. As a reminder, the damaged cross-section is from x=14” to x=14.125”.

This range would apply to all damage states, including the possibility of 5% damage. The higher damage states would be able to be identified almost anywhere on the plate; however, realistically, 50% damage should be noticed visibly and without the need for an involved method such as this one. Therefore, identifying this range would give the greatest chance to detect the damage states that wouldn’t be obvious, which is one of the underlying goals of this investigation.

5.3 Experimental Study

The experimental data was used to validate the analytical tests, and the best way to compare the experimental and analytical data was the bar graphs plotted for strain sensors at x=12.5”, x=14.5”, and x=16.5”. Both showed a similar pattern; the intensity of the integration was inversely related to the percentage of damage. They also both showed a steeper difference between the damage states’ intensity as the damage increases. This similar behavior was enough to validate the trends in the analytical model. However, the analytical data displayed a much smoother shape than the experimental data.

The biggest difference between the analytical and experimental signals was the amplitude at the natural frequency. For the analytical data, the maximum amplitude reached nearly 15 db. This was roughly 3.5 times greater than the experimental data’s highest amplitude of about 4db, found in the healthy state at sensor 2. This discrepancy, also displayed in the bar graphs, can most likely be attributed to the sensitivity of the foil gauges. Foil gauges, such as the ones used in the experiments, are somewhat insensitive. This causes the amplitude to decrease. However, they do share a similarity in the relationship they have with data from each sensor. For example, both the analytical and experimental bar graphs show the greatest magnitude to occur at sensor 2. The second

greatest is at sensor 1, with sensor 3 have the lowest magnitude for both. Because sensor 2 is the closest to the damage, it is reasonable for both tests to show this pattern.

There were several sources of error to consider when analyzing the data. Of course, any source of noise could cause an error or data distortion. Other sources include the installation of the strain gauges and temperature differences. When the strain gauges were installed, this allowed a possibility of human error. The gauges were uniaxial, so they needed to all be properly aligned; a slight change could cause a discrepancy in the strain reading. The cementing of the gauges is also important in order to ensure similar deformation to the plate [16]. As the cement dries and ages, the bond could weaken or harden, thus introducing noise into the system. For the given testing, one strain gauge had to be replaced solely for this reason. A solution for this would be to complete testing as quickly as possible after the installation. Change in temperature could also affect the strain readings. However, because it was a lab setting, the temperature remained fairly constant throughout testing. Also, foil gauges are less susceptible to error from temperature compared to other strain gauge types [20].

In conclusion, the experimental tests were able to validate the analytical data in two ways: the location of the natural frequency and the relationship between damage states. This validation of the analytical data by these experiments allowed the parametric study to continue. Although the amplitudes of the natural frequencies weren't similar, the discrepancy was attributed to poor sensitivity by the strain gauges. Using semiconductor strain gauges instead of foil gauges would most likely have a positive impact on the issue.

5.4 Advantages/Disadvantages of Strain Gauges

Noise distortion could be considered one of the main drawbacks in using strain gauges to VBDD. Others include the installation and longevity of the gauge, the variations of the gauges, and the restrictions on detection.

Compared to accelerometers, a strain gauge is more difficult and tedious to install. For an accelerometer, all that is required is for a hub to be glued securely to the specimen. After the installation of the hub, which is often magnetic as well, the accelerometer is secured to the hub and the installation is complete. For strain gauges, it is often a process that may take between 10-30 minutes, depending on the skill of the installer, and one that requires a variety of tools. This involved process is due to the extensive cleaning and smoothing needed to ensure as secure of a bond as possible to the specimen. An improper bond, due to poor cleaning, alignment, or cementing, can cause enough noise in the gauge to render it impractical to use. Even with a proper initial bond, the cement may decay or harden over time. This leads to increase noise in the system. Also, the fragility of the gauge must be considered; lead wires are very small diameter copper wires, and are very easy to detach from the gauge.

Proper installation is one of the main ways to avoid noise in the system. However, other sources do arise. For example, the lead wires traveling from the strain gauge to the data acquisition box always provide a source of noise, albeit small. This is due to the natural resistance in the wire which affects the resistance reading from the strain gauge. Improper grounding is another common source of noise. When all sources are combined, it has been found that that noise does have an effect on strain FRF signals. Previous research has stated that the amplitudes of FRF signals experienced both losses and gains, with amplitudes changing as much as 8 db [16].

The final area that strain gauges have a significant disadvantage to other transducers is the ability of global damage detection. Both accelerometers and displacement transducers work well for detecting global damage, but strain gauges are only truly useful in local damage detection [5]. This inability is due to the lack of a change in measureable strain far from the damaged area. Strain FRF signals only change noticeably when high strain occurs nearby, such as with a damaged area. Therefore, it could be useful to combine the two methods to achieve a complete damage detection

method [5]. In order to achieve an increase in global detection abilities, though still far less than accelerometers, semiconductor strain gauges may be chosen. As was mentioned previously, these sensors have a much higher gauge factor. This higher sensitivity means the sensor can detect smaller strains, which in turn means the detection of a larger spectrum of frequencies. Normal foil gauges are accurate only on lower frequencies, a disadvantage compared to other transducers. However, this increased sensitivity comes with a cost; semiconductor gauges are much more susceptible to temperature changes [20].

Strain gauges do have several advantages, though, that make them appealing for VBDD. One of the major advantages compared to accelerometers is the material cost. According to Omega Engineering, Inc., a low-cost accelerometer costs around 300 USD. For a strain uniaxial foil strain gauge from the same company, the cost is around 5 USD per gauge [22].

Accelerometers also are not able to measure some data that is available with strain gauges. For example, accelerometers are only able to detect damage dynamically. Strain gauges, however, can detect both dynamically and statically. Also, strain can be detected in pseudo-static loads, which make strain sensors more appealing for low-frequency excitations.

The main advantage for strain gauges is their increased ability to detect local damage compared to other types of transducers [4] [5] [16]. It has been shown that near a crack or other changes in stiffness, the FRF signals from strain data change much more than from acceleration or displacement data. Again, this makes it practical to combine multiple types of transducers to successfully detect damage.

5.5 Future Work

Using this study as a basis, future work could expand on the experimental side of this investigation. Strain gauges with higher resolution placed in more locations would

allow a parametric study using experimental data. Also, this study should be able to help researchers decide the placement of strain gauges experimentally. Because high stress/strain areas can be located beforehand using finite element models, and damage can be detected globally using accelerometer data, strain gauges can be effective in accurately measuring local damage. Ideally, this method would be used in combination with other methods, as mentioned in previous sections, to increase the overall capability of a damage-detection system. Accelerometers and strain gauges have strengths that would complement each other well in a compiled method. Thus, there would be both global damage detection from accelerometer FRF signals and local damage detection using strain FRF signals.

5.6 Conclusion

This study was completed in order to investigate the effective range of strain gauges for vibration-based damage detection. It was found that strain gauges were able to detect damage in a plate using a version of the frequency response function method. The method was able to detect if damage was present, and then quantify each level of damage relative to the healthy state. Also, an effective range for the strain gauges with this method was able to be determined. Data for the parametric investigation was found analytically while experiments were being conducted in a laboratory setting simultaneously. Although the experimental data did not correlate exactly with the analytical data, most noticeably with the magnitude of the FRF signals, the basic trend of the natural frequency's amplitude decreasing as damage increased was the same for both. Therefore, it was considered to validate the analytical data.

APPENDIX

The following table lists the location of each sensor for the parametric test. The distances given are from the end closest to the impact area. Figure 13 visually lays out the location of each sensor. The blue boxes correspond to the three sensors used in the damage detection method and the analytical tests. The beige boxes indicate the sensors on either side of the damage.

Table A1: A list of locations for each of the sensors used in the parametric tests.

x [in]	Sensor #
26.5	Reference
1	1
1.5	2
2	3
2.5	4
3	5
3.5	6
4	7
4.5	8
5	9
5.5	10
6	11
6.5	12
7	13
7.5	14
8	15
8.5	16
8.75	17
9	18
9.25	19
9.5	20
9.75	21
10	22
10.25	23
10.5	24
10.75	25
11	26
11.25	27
11.5	28
11.75	29
12	30

(continued)

x [in]	Sensor #
12.125	31
12.25	32
12.375	33
12.5	34
12.625	35
12.75	36
12.875	37
13	38
13.125	39
13.25	40
13.375	41
13.5	42
13.625	43
13.75	44
14.25	45
14.375	46
14.5	47
14.625	48
14.75	49
14.875	50
15	51
15.125	52
15.25	53
15.375	54
15.5	55
15.625	56
15.75	57
15.875	58
16	59

(continued)

x [in]	Sensor #
16.25	60
16.5	61
16.75	62
17	63
17.25	64
17.5	65
17.75	66
18	67
18.25	68
18.5	69
18.75	70
19	71
19.25	72
19.5	73
19.75	74
20.25	75
20.75	76
21.25	77
21.75	78
22.25	79
22.75	80
23.25	81
23.75	82
24.25	83
24.75	84
25.25	85

BIBLIOGRAPHY

[1] C. R. Farrar and D. A. Jauregui, "Comparitive Study of Damage Identification Algorithms Applied to a Bridge: I. Experiment," *Smart Mater,* pp. 704-719, 1998.

[2] S. W. Doebilng, C. R. Farrar and M. B. Prime, "A Summary Review of Vibration-Based Damage Identification Methods," Los Alamos National Labaratory, Los Alamos, NM.

[3] R. Sampaio, N. Maia and J. Silva, "Damage Detection Using the Frequency-Response-Function Curvature Method," *Journal of Sound and Vibration,* pp. 1029-1042, 1999.

[4] Y. Chen and A. Swamidas, "Change of modal parameters due to crack growth in a tripod tower platform," *Canadian Journal of Civil Engineering, 20,* pp. 801-803, 1993.

[5] A. S. J. Swamidas and Y. Chen, "Monitoring the Crack Growth Through Change of Modal Paramaters," *Journal of Sound and Vibration,* pp. 325-343, 1995.

[6] D. O. Bernasconi and P. D. Ewins, "Application of Strain Modal Testing to Real Structures," *7th Internation Modal Analysis Conference,* pp. 1453-1464, 1989.

[7] S. Jang, S.-H. Sim and B. Spencer Jr., "Structural Damage Detection Using Static Strain Data," University of Illinois at Urbana-Champaign, 2008.

[8] L. Wang and T. H. Chan, "Review of vibration-based damage detection and condition assessment of bridge structures using structural health monitoring," in *The Second Infrastructure Theme Postgraduate Conference*, 2009.

[9] D. J. Inman, Engineering Vibration, Saddle River, NJ: Prentice Hall, Inc., 1996.

[10] C. W. d. Silva, Vibration: Fundamentals and Practice (Second Edition), Boca Raton, FL: Taylor and Francis Group, 2007.

[11] W. G. Halvorsen and D. L. Brown, "Impulse Technique for Structural Frequency Response," *Journal of Sound and Vibration,* November 1977.

[12] C. Cai, H. Zheng, M. Khan and K. Hung, "Modeling of Material Damping Properties in ANSYS," Defense Systems Division, Institute of High Performance Computing, Singapore.

[13] K. He and W. Zhu, "Structural Damage Detectiong Using Changes in Natural Frequencies: Theory and Application," in *9th International Conference on Damage*

Assessment of Structures, 2011.

[14] P. J. Cruz and R. Salgado, "Performance of Vibration-Based Damage Detection Methods in Bridges," *Computer-Aided Civil and Infrastructure Engineering,* vol. 24, pp. 62-79, 2008.

[15] L. Yam, T. Leung, D. Li and K. Xue, "Theoretical and Experimental Study of Modal Strain Analysis," *Journal of Sound and Vibration,* pp. 251-260, 1996.

[16] L. Vari and P. Heyns, "Strain modal testing - a critical appraisal," *R&D Journal, vol. 13, no. 3,* pp. 83-90, 1997.

[17] ANSYS, Inc., "Ansys 14.0 Help," SAS IP, Inc., 2011.

[18] C. J. Schallhorn, "Localization of Vibration-Based Damage Detection Method in Structural Applications," University of Iowa, Iowa City, IA, 2012.

[19] University of California, Berkley Computers & Structures, Inc., "Damping and Energy Dissipation: Linear Viscous Damping is a Property of the Computer Model and is Not a Property of a Real Structure," [Online]. Available: www.csiberkeley.com/system/files/technical-papers/19.pdf.

[20] Omega Engineering, Inc., "Omega," 2013. [Online]. Available: http://www.omega.com/literature/transactions/volume3/strain.html#sendes. [Accessed March 2013].

[21] A. Swamidas and Y. Chen, "Monitoring Crack Growth Through Change of Modal Parameters," *Journal of Sound and Vibration,* vol. 186, no. 2, pp. 325-343, 1995.

[22] Omega Engineering, Inc., "Accelerometers/Strain Gauges," 2013. [Online]. Available: http://www.omega.com/pptst/ACC101.html, http://www.omega.com/ppt/pptsc.asp?ref=SGD_LINEAR1-AXIS&ttID=SGD_LINEAR1-AXIS&Nav=. [Accessed March 2013].

[23] T. Irvine, "Bending Frequencies of Beams, Rods, and Pipes," 20 November 2012. [Online]. Available: www.vibrationdata.com/tutorials2/beam.pdf.

[24] R. D. Adams, P. Cawley, C. J. Pye and B. J. Stone, "A Vibration Technique for Non-Destructively Assessing the Integrity of Structures," *Journal of Mechanical Engineering Science,* pp. 93-100, April, 1978.